MECHANISMS OF ION AND LIPID TRANSPORT BY RECONSTITUTED TMEM16 PROTEINS

A Dissertation

Presented to the Faculty of the Weill Cornell Graduate School

of Medical Sciences

in partial Fulfillment of the Requirements for the Degree of

Doctor of Philosophy

By

Mattia Malvezzi

May 2016

MECHANISMS OF ION AND LIPID TRANSPORT BY RECONSTITUTED TMEM16 PROTEINS

Mattia Malvezzi, Ph.D.

Cornell University, 2016

Phospholipid scrambling, the process by which cells collapse the lipid asymmetry on the plasma membrane, causes phosphatidylserine (PS) to be exposed to the outer leaflet of the plasma membrane, triggering blood coagulation and marking apoptotic cells. TMEM16 proteins were originally thought to be ion channels, but it quickly became clear that this family of membrane proteins was characterized by a high degree of functional divergence when other members were suggested to be Ca^{2+}-dependent phospholipid scramblases. These findings created a controversy in the field, especially around the function of TMEM16F which was reported to be an ion channel, a phospholipid scramblase and both. To solve this controversy we decided to take a biochemical approach, aiming to purify TMEM16 members for functional reconstitution into artificial membranes. We identified a novel TMEM16 homologue, afTMEM16 from the fungus *Aspergillus fumigatus*, which is a dual function, Ca^{2+}-dependent channel/scramblase where the two functions are regulated by the same Ca^{2+}-binding site. This was the first direct evidence that

TMEM16 members are indeed phospholipid scramblases and that TMEM16s can be dual function proteins. Shortly after, the crystal structure of a fungal TMEM16 phospholipid scramblase, nhTMEM16, was solved by the Dutzler group. The structure provided the basis for a first mechanistic hypothesis on lipid translocation: interactions between the headgroup of a phospholipid and residues within a 8-11 Å wide cavity at the protein-lipid interface would allow lipids to get translocated across the membrane in a semicircular, bi-directional fashion. We decided to begin testing this hypothesis by investigating how lipids of increasing headgroup size are scrambled in the presence and absence of Ca^{2+}. We found that in the Ca^{2+}-bound state the headgroup size cut off is considerably larger than the width of the cavity, suggesting that tight interactions between the lipid headgroup and the cavity are not required for scrambling. Interestingly, we found that the apo-state conductance has a similar cut off than that of the Ca^{2+}-bound state, suggesting the presence of one conductive state where the apo state can visit the open conformation even in the absence of Ca^{2+}.

BIOGRAPHICAL SKETCH

Dr. Malvezzi's interests focus on membrane transport and the structural and functional mechanisms underlying the movement of molecules across biological membranes. Membrane proteins play a crucial role in physiological processes, ranging from generation and transmission of electrical signals, epithelial secretion and sensory transduction to blood coagulation and apoptosis. Understanding the mechanism by which membrane proteins allow for transport of specific molecules is crucial also for a better understanding of the pathological conditions related to malfunctions of specific proteins.

Educational background:

February 2010-Feb 2016 Graduate Student (transfer from U. of Iowa)
Weill Cornell Graduate School of Medical Sciences, New York, NY.
Physiology, Biophysics and Systems Biology (PBSB) program
Thesis Advisor: Dr. Alessio Accardi, Ph.D.

August 2009 – December 2010 Graduate Student
University of Iowa, Iowa City, IA.
Molecular Physiology and Biophysics program.
Thesis Advisor: Dr. Alessio Accardi, Ph.D.

January 2008 – July 2009 Exchange Student
University of Iowa, Iowa City, IA.
Department of Molecular Physiology and Biophysics.
Supervisor: Dr. Alessio Accardi, Ph.D.

September 2002 – October 2007 Bachelor of Science (Biotechnology)
University of Modena and Reggio-Emilia, Modena, MO, Italy.
Thesis Advisor: Dr. Paolo Facci, Ph.D

This thesis is dedicated to my family: my mother, Giuliana; my father, Paolo and my brother, Riccardo, for their constant and unconditioned support.

It is also dedicated to my dearest friends: Alberto, Daniele, Emiliano and Davide.

ACKNOWLEGMENTS

I would like to acknowledge my supervisor, Dr. Alessio Accardi, for his incredible help and support throughout my career as a student and for his invaluable contribution to my growth as a scientist.

I would like to acknowledge all the people who worked with me during these years in the lab for their help and passion, for our scientific discussions and for making working in the lab and incredibly enjoyable experience.

I would like to acknowledge the Graduate School, the Physiology, Biophysics and Systems Biology program and all the students, faculty and staff.

I would like to acknowledge the grants that allowed this research to be conducted from the NIH and Irma T. Hirschl/ Monique Weill-Caulier Scholar Award.

TABLE OF CONTENTS

LIST OF FIGURES

LIST OF TABLES

LIST OF ABBREVIATIONS

BSA : bovine serum albumin

CaCC : Ca^{2+}-activated Cl^- channel

DAG : Dacylglycerol

DIDS : 4,4'-Diisothiocyano-2,2'-stilbenedisulfonic acid

EGTA : ethylene glycol tetraacetic acid

ER : Endoplasmic Reticulum

IP_3 : Inositol trisphosphate

NA : Niflumic Acid

NBD : nitrobenzoxadiazole

NMDG : N-Methyl-D-glucamin

NPA : N-phenylanthranilic acid

PC : Phosphatidylcholine

PEG : *Polyethylene glycol*

PI : Phosphatidylinositol

PIP_2 : Phosphatidylinositol 4,5-bisphosphate

PKC : Protein Kinase C

POPE : 1-palmitoyl-2-oleoyl-*sn*-glycero-3-phosphoethanolamine

POPG : 1-palmitoyl-2-oleoyl-*sn*-glycero-3-phospho-(1'-*rac*-glycerol)

PS : Phosphatidylserine

SDS-PAGE : sodium dodecyl sulfate-polyacrylamide gel electrophoresis

SLACK : sequence like A calcium-activated K^+ channel

SM : Sphyngomyelin

TEA : Tetraethylammonium

1. Summary

Phospholipid scrambling, the process by which cells collapse the lipid asymmetry on the plasma membrane, causes phosphatidylserine (PS) to be exposed to the outer leaflet of the plasma membrane, triggering blood coagulation and marking apoptotic cells. Although this process has been known since the 1970s the molecular identity of Ca^{2+}-dependent phospholipid scramblases, the proteins responsible for translocating lipids between leaflets, has remained elusive until recently when it was shown that members of the TMEM16 family are the long-sought molecular counterpart of Ca^{2+}-dependent phospholipid scramblases. TMEM16 proteins were originally thought to be ion channels, as TMEM16 A and B were shown to be Ca^{2+}-activated Cl^- channels but it quickly became clear that this family of membrane proteins was characterized by a high degree of functional divergence when other members were suggested to be Ca^{2+}-dependent phospholipid scramblases. These findings created a controversy in the field, especially around the function of TMEM16F which was reported to be an ion channel with multiple gating properties and selectivities or a phospholipid scramblase with no channel activity. While the conclusion that TMEM16F is involved in phospholipid scrambling was confirmed by independent groups, the question of whether TMEM16F, and by extension other TMEM16 homologues, was a phospholipid scramblase itself, an ion channel regulating unknown scramblases or perhaps a dual function channel/scramblase remained open. To come to a definitive answer to this question we decided to take a biochemical approach, aiming to purify TMEM16 members for functional

reconstitution into artificial membranes. We reasoned that this would allow us to directly test whether any TMEM16 proteins were phospholipid scramblases without the complications associated to the heterologous overexpression of a protein with unknown function in cells (i.e. altering expression of different proteins and cellular components, altering trafficking). We identified a novel TMEM16 homologue, afTMEM16 from the fungus *Aspergillus fumigatus*, which is a dual function, Ca^{2+}-dependent channel/scramblase where the two functions are regulated by the same Ca^{2+}-binding site. This was the first direct evidence that TMEM16 members are indeed phospholipid scramblases and that TMEM16s can be dual function proteins. Interestingly, in agreement with our results, it was recently shown by two independent groups that TMEM16F is a dual function channel/scramblase as well, suggesting that all the previous studies might have captured only one of the two functions.

Shortly after, the crystal structure of a TMEM16 phospholipid scramblase was solved by the Dutzler group, identifying the lipid translocation pathway and starting to unveil the mechanism by which phospholipid scramblases work. The structure of nhTMEM16, a fungal homologue from *Nectria haematococca,* provided the basis for a first mechanistic hypothesis on lipid translocation: interactions between the headgroup of a phospholipid and residues within a 8-11 Å wide cavity at the protein-lipid interface would allow lipids to get translocated across the membrane in a semicircular, bi-directional fashion. We decided to begin testing this hypothesis by investigating how lipids of increasing headgroup size are scrambled in the presence and absence of Ca^{2+}. We found that in the

Ca^{2+}-bound state the headgroup size cut off is considerably larger than the width of the cavity, suggesting that tight interactions between the lipid headgroup and the cavity are not required for scrambling. To begin probing the conformational changes occurring upon Ca^{2+} binding we took advantage of the fact that afTMEM16, like nhTMEM16, scrambles lipids even in the absence of Ca^{2+}. Interestingly, we found that this apo-state conductance has a similar cut off than that of the Ca^{2+}-bound state, suggesting the presence of one conductive state where the apo state can visit the open conformation even in the absence of Ca^{2+}.

2. Introduction

2.1. Phospholipid scrambling

Membrane bilayers delimit and compartmentalize all living cells. In eukaryotes, lipid biogenesis occurs in the endoplasmic reticulum (ER) where lipids are randomly distributed between the two leaflets of the membrane. As lipids travel downstream from the ER, via the Golgi apparatus, to reach the plasma membrane, the lipid composition of the membranes becomes progressively asymmetric. The result is the specific asymmetric lipid composition of plasma membranes found in all living cells (**Figure 1A**). In eukaryotes, choline-containing phospholipids (phosphatidylcholine, PC and sphyngomyelin, SM) are more abundant on the outer leaflet while amino phospholipids phosphatidylethanolamine (PE), phsophatidylserine (PS) and phosphoinositides (such as PI and PIP_2) are confined to the inner leaflet of the membranes (**Figure 1A)**, contributing to generate the negative membrane potential found in most cells. This asymmetry is generated and maintained by two classes of lipid-translocating, ATP-driven enzymes that move lipids across the membranes against their concentration gradients at the cost of ATP: flippases and floppases. These enzymes are lipid specific: flippases catalyze the transfer of PE and PS from the outer to the inner leaflet, viceversa floppases move PC and SM from the inner to the outer leaflet (**Figure 1B**). The identity of flippases and floppases is known and includes P4 ATPases and ABC transporters [1 2 3 4 5 6,7]. As observed for other active transport events, the rate of lipid transport is relatively slow with half times of minutes or less [8 9].

Maintenance of this lipid asymmetry is crucial for the cell homeostasis and many physiological processes. Many signal transduction pathways use phosphoinositides which are predominant on the inner leaflet of the membrane. For example, Phosphatidylinositol 4,5-bisphosphate (PIP_2) cleavage to Inositol trisphosphate (IP_3) and Dacylglycerol (DAG) initiates Ca^{2+}-release from intracellular stores and Protein Kinase C (PKC) activation which regulates a variety of intracellular cascades involved in receptor desensitization, transcription regulation, cell growth regulation, learning and memory. Although maintaining the lipid asymmetry is crucial for living cells, rapid loss of phospholipid asymmetry is an equally important physiological process, known as phospholipid scrambling. As lipids are signaling molecules, by changing the relative abundance of lipids in both leaflets cells regulate a variety of physiological processes. Ca^{2+}-dependent phospholipid scramblases are a third class of lipid-moving proteins responsible for collapsing the lipid asymmetry on the plasma membrane. The process of creating and maintaining the lipid asymmetry is fundamentally different from phospholipid scrambling, and this is reflected by key differences between the two classes. Unlike flippases/floppases, scramblases have to move lipids rapidly and bi-directionally re-equilibrating their chemical gradients, are non-specific for lipids and do not require ATP but instead by Ca^{2+} [10] (although it has been shown that some Ca^{2+}-independent scramblases exist[11] (**Figure 1B**). The most important consequence of phospholipid scrambling is the exposure of PS, normally sequestered to the cytoplasmic leaflet, to the outer leaflet of the membranes which triggers blood coagulation and marks apoptotic cells. In platelets, PS exposure is

a pro-coagulant factor as blood clotting complexes bind to PS initiating a series of molecular events resulting in the formation of fibrin clots (**Figure 2A**)[10,12] PS externalization is also a marker of apoptotic cells, as on the outer leaflet it functions as one of the ‘’eat me’’ signals for phagocyte recognition and the suppression of inflammatory responses (**Figure 2B**)[13], although it has been shown to be required but not sufficient for phagocyte recognition[14] .Blood coagulation and apoptotic cell recognition are the two best-described physiological consequences of PS exposure, but there are other, less well-characterized processes where PS exposure plays a key role. For example, transient PS exposure has been shown to be essential in cell fusion events occurring during myotube formation in muscle cell differentiation[15]. It is important to notice that PS also has significant but different features when confined to the inner leaflet of the membrane, where it helps organizing lipid rafts, recruits specific complexes that facilitate endocytosis, trafficking and vesicle formation, recruits signaling molecules such as PKC, Ras and Src[16]. Therefore, controlling the abundance of PS on both leaflets is essential for the physiology of eukaryotic cells.

The role of Ca^{2+} in phospholipid scrambling has been established from the late 1980s[17,18]. Ca^{2+} ionophores, such as ionomycin, were used to show loss of lipid asymmetry caused by increased intracellular Ca^{2+} levels in several hematopoietic cell types, including erythrocytes and blood cells from Scott Syndrome patients. Ca^{2+} has been shown to be crucial for phospholipid scrambling during apoptosis but, unlike blood clot formation, it is not always required for activating the scramblases[19,20].

Even though the process of phospholipid scrambling has been known since the 1970s, the molecular identity of phospholipid scramblases has been only recently identified, when members of the newly-discovered TMEM16 family of membrane proteins were shown to be phospholipid scramblases. Before identifying members of the TMEM16 family as scramblases, few false positives were discovered, particularly hPLSCR1[21,22] and ABCA1, a member of the ATP-Binding-Cassette (ABC) transporters [23] which were shown not to be phospholipid scramblases after initial reports seemed to suggest otherwise.

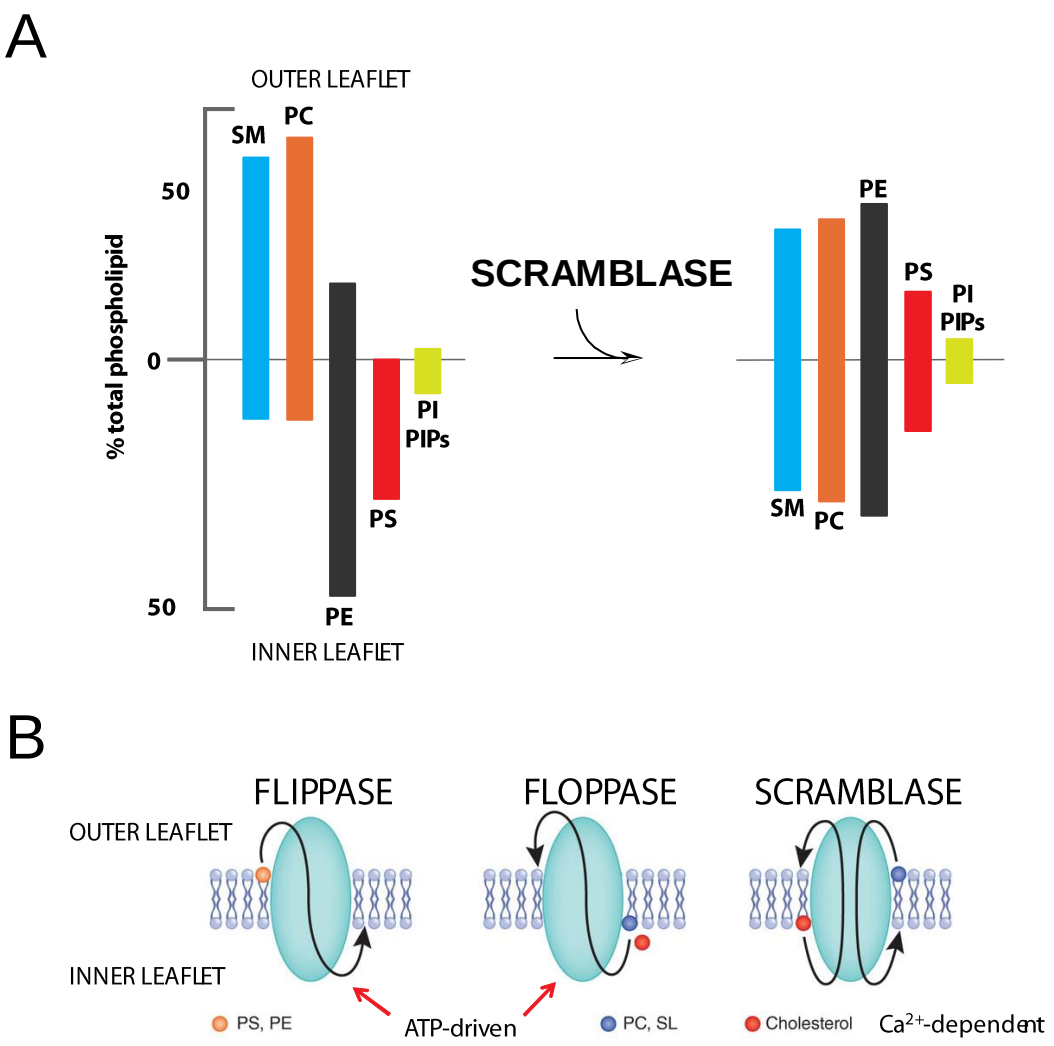

Figure 1: Phospholipid scrambling.
A: The lipid composition of all cell membranes is asymmetric and upon activation of scramblases the asymmetry collapses. A typical erythrocyte membrane lipid composition is shown (SM: Sphingomyelin; PC: phosphatidylcholine; PE: phosphatidylethanolamine; PS: phosphatidylserine; PI: phosphatidylinositol; PIPs: phosphoinositides). **B**: Classification of lipid-moving enzymes. Flippases and floppases move lipids unidirectionally against their concentration gradient, they are lipid-specific and ATP-dependent. Scramblases move lipids bidirectionally along their concentration gradient with no lipid specificity and they are activated by Ca^{2+} [1].

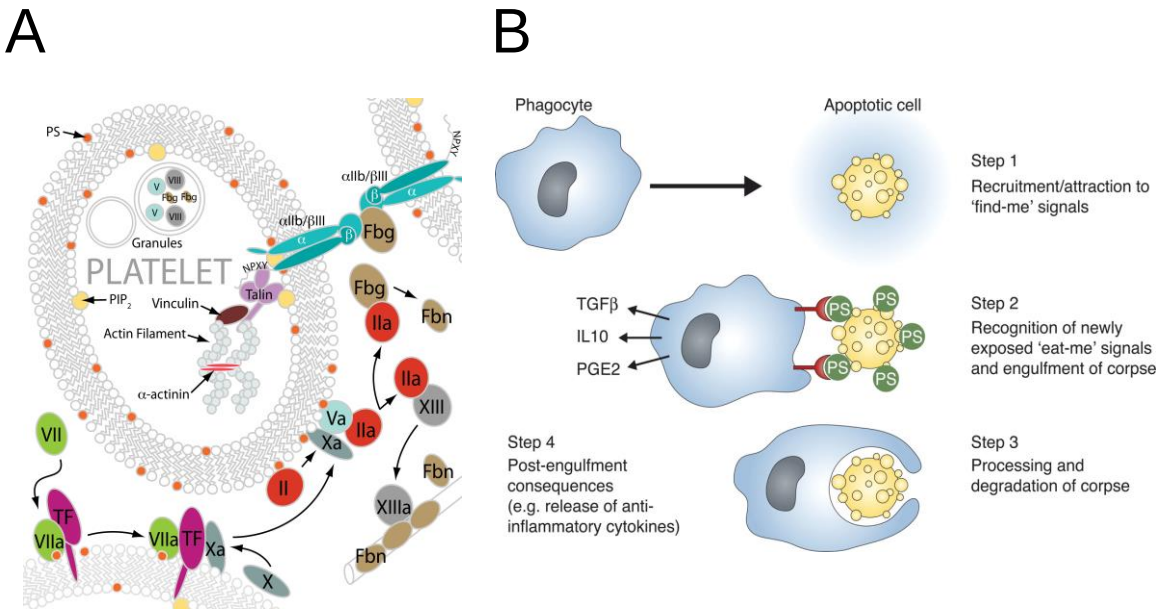

Figure 2: Roles of phosphatidylserine during blood coagulation and apoptosis.
A: In platelets, phosphatidylserine (PS) exposure is a pro-coagulant factor as blood clotting complexes bind to PS initiating a series of molecular events resulting in the formation of fibrin clots. Trauma activates factor VIIa (FVIIa), which binds tissue factor (TF) to initiate the extrinsic blood clotting cascade. FVIIa binding is dependent on PS. (figure from http://www.scs.illinois.edu/rienstra/research/struct_bio.html). **B**: The ''find-me'' signals (such as low levels of nucleotides ATP and UTP or sphingosine 1-phosphate) released by apoptotic cells help attract motile phagocytes to the proximity of the cell undergoing apoptosis. The phagocytes then use engulfment receptors on their surface to engage ''eat-me signals'' on apoptotic cells. PS acts as one of the ''eat-me'' signals for phagocyte recognition (figure from [24]).

2.2. TMEM16 family: Ca^{2+}-gated channels, Ca^{2+}-dependent scramblases and more

The TMEM16 family, also known as Anoctamins (Ano), comprises 10 human members (TMEM16A-K, I is omitted, corresponding to Ano 1-10) (**Figure 3**). Interestingly, no TMEM16 orthologues are found in bacteria. The family is characterized by a high degree of functional divergence, as it comprises at least Ca^{2+}-activated Cl^- channels, phospholipid scramblases and dual function channel/scramblase proteins. It is known that TMEM16 A and B are CaCCs[25-27,28] but the functions of many TMEM16s is still unknown or controversial. The best example of this is the fact that TMEM16F has been suggested to be a Ca^{2+}-gated channel[29,78,89], a phospholipid scramblases[29] and a dual function channel/scramblase[30,31]. TMEM16 C, D, G and J were proposed to be phospholipid scramblases[32], as well as the fungal homologue nhTMEM16[33]. Finally, we showed that the fungal afTMEM16 is a dual function channel/scramblase.

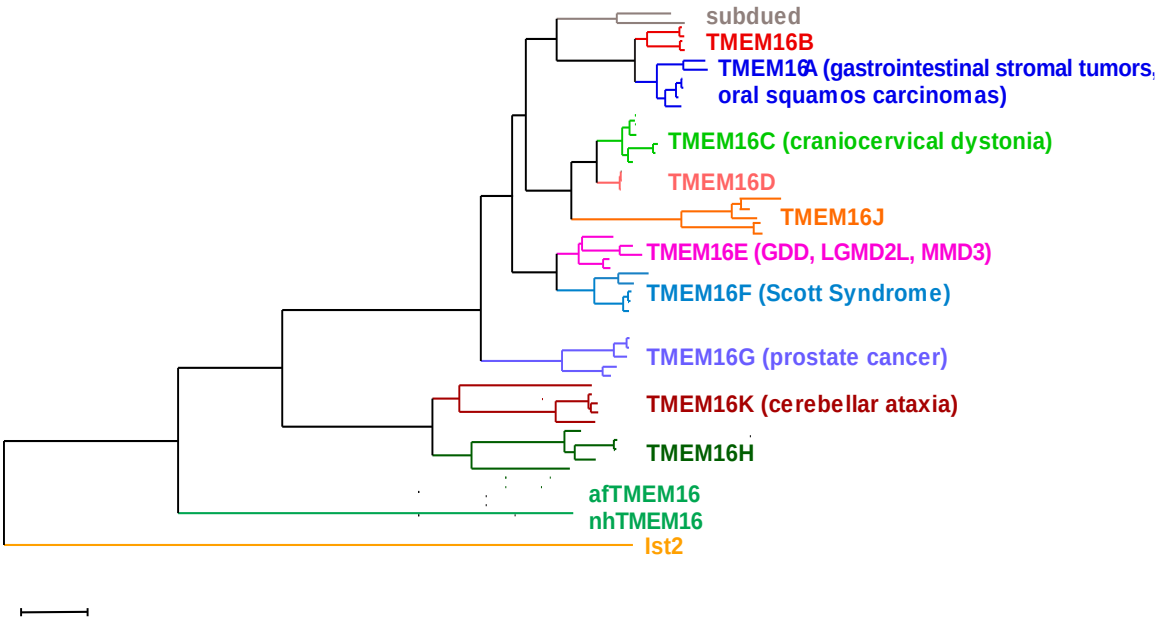

Figure 3: Phylogeny of TMEM16 proteins.
Sixty TMEM16 protein sequences were obtained from the PFAM database from Mammalia (30), Actinopterygii (13), Arthopoda (10), Fungi (3) and no kingdom (4). Multiple sequence alignment was performed using CLUSTALW. From this initial alignment, the five most divergent sequences were removed and a new alignment was built. Phylogenetic analysis was conducted using PhyML 3.0[34] and the phylogenetic tree was built using SeaView[35] . Scale bar indicates one nucleotide substitution per site. Diseases related to each member are indicated (*see List of abbreviations*). To avoid confusion the *Anoctamin* nomenclature is omitted. (adapted from[36])

2.2.1. Pathology of TMEM16s

TMEM16 proteins have been implicated in a variety of different diseases. Although these diseases are different and affect various cellular processes, they are all linked to either membrane-related defects or alteration of Ca^{2+}-signaling. This is consistent with the Ca^{2+}-dependent scrambling activity proposed for some of the TMEM16 proteins. The best example of pathophysiological correlations between TMEM16 proteins and their involvement in phospholipid scrambling comes from the observation that mutations in the TMEM16F gene are associated with Scott Syndrome[29,37,38], a rare bleeding disorder where cells fail to expose PS on the outer leaflet of the membrane preventing blood clotting. Specifically, it was shown that a patient with Scott Syndrome carried a mutation at a splice sit resulting in premature termination of the protein[29]. As TMEM16F has been suggested to be a phospholipid scramblase, this explains the PS exposure associated with Scott Syndrome.

Mutations in TMEM16E (the gene was called GDD1 at the time) were shown to be associated with gnathodiaphyseal dysplasia (GDD), a rare dominant skeletal syndrome characterized by reduced bone mineral density (osteopenia), which causes the bones to be unusually fragile[39,40] . Because of protein localization and topology, the authors hypothesized that GDD1 might function as an intracellular channel of the ER membrane involved in the Ca^{2+}-dependent signaling pathway, and that mutations induce excess Ca^{2+} release from the ER. Interestingly, TMEM16E is expressed in growth-plate chondrocytes and osteoblasts at the sites of active bone turnover[39]. This not only suggests a role in

bone formation, but also that, given that PS exposure is important during bone repair[41], TMEM16E might be directly involved in PS exposure. Mutations of TMEM16E are also associated with two different muscular dystrophies: proximal limb-girdle muscular dystrophy (LGMD2L) [42,43] and distal Miyoshi myopathy (MMD3)[44]. The resulting phenotypes are all characterized by defective skeletal muscle repair. TMEM16E has been shown to play a role in the maintenance of skeletal muscles[39], suggesting that it might be directly related to muscle membrane repair.

Mutations in TMEM16K were found to cause autosomal-recessive cerebellar ataxia[45-47], a form of ataxia (lack of voluntary coordination of muscle movements that includes gait abnormality) originating in the cerebellum which causes inability to coordinate balance, gait, and extremity and eye movements. TMEM16K is highly expressed in the cerebral cortex and in the cerebellum. Although it is not clear whether TMEM16K is a CaCC, this is an intriguing hypothesis as the most important mechanism causing cerebellar ataxia is disruption of Ca^{2+} signaling in Purkinje cells[48].

Mutations in TMEM16C were reported to cause a dominant form of craniocervical dystonia[49] in which sustained muscle contractions cause twisting and repetitive movements or abnormal postures. Although the mechanism of action of the mutations is not known TMEM16C is highly expressed in the striatum and facilitates Na^+-activated K^+ currents by SLACK[50], thus it is possible that alterations in TMEM16C function caused by the dominant mutations perturb the excitability of striatal neurons.

TMEM16 proteins are also involved in cancer. TMEM16A, a CaCC, was found to be highly expressed in gastrointestinal stromal tumors[51,52], amplified and over expressed in oral squamous cell carcinomas[53]. In most cases TMEM16A is over expressed in tumors due to gene amplification of the chromosomal locus (11q13) in which it is located[53]. Over expression of TMEM16A correlates with reduced survival and increased metastasis[54,55]. It seems that the role of TMEM16A is to increase cell proliferation and promote cell migration, as shown by in vitro knockdown or inhibition of TMEM16A[56]. TMEM16G (also known as NGEP), is highly expressed in prostate cancer[57,58]. It has been proposed that TMEM16G might be a phospholipid scramblase[32] and interestingly, it might also promote cell association[59]. Thus, given that PS exposure seem to promote cell-cell association, it is possible that over-expression of TMEM16G leads to abnormal fusion events driven by PS exposure.

2.2.2. TMEM16A and B: Ca^{2+}-activated Cl^- channels

Ca^{2+}-activated Cl^- channels (CaCCs) have been known for decades as key players in a variety of physiological processes. First described in the 1980s in the Xenopus oocytes, where they regulate fast block to polyspermy, and salamander photoreceptors[60-62], these channels are widely expressed and control epithelial secretion[63], membrane excitability in neurons and cardiac muscles[64,65], olfactory transduction[66], regulation of vascular tone[67], photoreception[68] and nociception[69] .Only in 2008 it was shown that members of the TMEM16 family encoded for the long sought CaCCs when three independent groups demonstrated that TMEM16A

is a CaCC with biophysical properties resembling those of native channels. Interestingly, they came to this conclusions by using three different approaches[25-27]. Definitive proof that TMEM16A is the pore-forming subunit of a CaCC came from our lab, as we were able to over-express, purify and functional reconstitute TMEM16A in artificial vesicles and showed it recapitulated the properties of native CaCCs[70].

TMEM16A is widely expressed and plays diverse key roles in many physiological processes. It regulates fluid transport in epithelia such as airway and salivary glands and vascular and smooth muscle contractility, it is expressed in dorsal root ganglion neurons where it is involved in nociception and it has a role in cell proliferation and metastasis[25,26,71-73]. Biophysical properties of TMEM16A resemble those of native CaCCs: outwardly-rectifying Cl^- current, Ca^{2+}- sensitivity in the low micromolar range, ion selectivity (NO_3^- > I^- > Br^- > Cl^- > F^-)[25,27,74], pharmacological profile of inhibition by canonical Cl^- channel blockers in the low μM range, including Niflumic Acid (NA), 4,4'-Diisothiocyano-2,2'-stilbenedisulfonic acid (DIDS) and N-phenylanthranilic acid (NPA) [25,70]. Ionic selectivity of TMEM16A has two important features compared to most channels: its anionic selectivity is not fixed but changes during channel activation[27] and its anion/cation selectivity is not strong with a P_{Cl^-}/P_{X^+} of only ~7 [25,75].

Ca^{2+} sensitivity of TMEM16A is in the sub-micromolar range, ~0.3-0.6 μM[25-27]. Although it is not possible to rule out that calmodulin might regulate TMEM16A, it is not required for function, as proved by the fact that purified TMEM16A functions as a CaCC and addition of calmodulin does not alter its

properties[76 70]. Work from several laboratories showed that a pair of conserved, negatively-charged amino acids in the third intracellular loop plays a key role in the Ca^{2+} sensitivity of several TMEM16 homologues, including TMEM16A[75,70,77].

Shortly after the identification of TMEM16A, TMEM16B was also shown to be a CaCC [28,78,79]. Despite being both CaCCs there are important differences between the two proteins. TMEM16B, unlike TMEM16A, has a less widespread expression and it is mostly expressed in sensory neurons where it regulates signal transduction in vision and olfaction[28,79]. The Ca^{2+}-sensitivity of TMEM16B, in the low micromolar range, is ~10 fold lower than that of TMEM16A[78]. Currents from TMEM16B heterologously expressed displays faster kinetics of activation and deactivation than TMEM16A[28,78,79]. These differences might be due to the different physiological processes TMEM16A and B are responsible for, as in an epithelial cells channels are likely to remain open more time than in a sensory neuron where transient signaling is required.

2.2.3. TMEM16F: a Ca^{2+}-gated channel, a Ca^{2+}-dependent phospholipid scramblase, a dual function protein

What is TMEM16F? To date, several reports on TMEM16F have been published and the overall picture emerging is confusing. Several lines of evidence suggest that TMEM16F is a Ca^{2+}-dependent phospholipid scramblase, particularly important during blood coagulation. The first report came in 2010 from the Nagata group[29]. By expression cloning they identified a B-cell line, Ba/F3, where PS exposure was detected after treatment with the Ca^{2+} ionophore. Ionophore-

stimulated cells derived from a patient affected by Scott syndrome, a rare bleeding disorder, did not display PS exposure, consistent with the hypothesis of having impaired scrambling caused by TMEM16F mutations. This was the first evidence linking TMEM16F as a protein involved in Ca^{2+}-dependent phospholipid scrambling. Several other papers then supported the hypothesis of TMEM16F, as well other TMEM16 proteins, as phospholipid scramblases [14,32,80,81]. Putative scrambling activity by TMEM16F has been associated not only with blood clotting formation but also apoptosis, although it seems it is required but not sufficient for the cells to be recognized by macrophages [14,81], and bone mineralization[82,83].

While these studies suggested a role for TMEM16F in phospholipid scrambling, they could not discriminate whether it was a regulator of an unknown scramblases or a scramblase itself. This problem was compounded by the numerous reports suggesting that TMEM16F is an ion channel and not a scramblase. Interestingly, these reports did not agree on what type of ion channel: a volume-regulated Cl^- channel[84], an outwardly-rectifying Cl^- channel[85], a Ca^{2+}-activated Cl^- channel[86-89] and a Ca^{2+}-activated channel permeable to cations[77]. Furthermore, many of these studies directly contradicted each other. For example, some reports indicated that TMEM16F did not contribute to volume-regulated currents [89]or that it is not a phospholipid scramblase per se but an essential component for lipid scrambling in platelets during blood coagulation[77].

Taken together these results are confusing and cannot be simultaneously correct. It is hard to understand how it is possible to have such different results

with the same protein. These inconsistencies cannot be simply ascribed to the use of different expression systems or experimental approaches: in many cases nominally identical cell lines, clones and techniques are utilized. One possibility is that the overexpression of TMEM16F has pleiotropic effects on the expression and/or trafficking of many different channels and scramblases in cells and that slight differences in the experimental procedures (i.e., transfection techniques, assay details, solution composition, [Ca^{2+}] used) might underlie these divergent results. Furthermore, it seems that TMEM16F-dependent scrambling represents only one way by which cells externalize PS and a TMEM16F-indipendent pathway might be present during blood coagulation and apoptosis. This might explain some of the results that suggested that channel activity of TMEM16F is not required to have complete scrambling and the reduced but not abolished scrambling in TMEM16F $^{-/-}$ cells/animals because the presence of a TMEM16F-indipendent scrambling pathway will not be influenced by blocking/knocking down TMEM16F[80]. Another explanation would be that TMEM16F is able to move ions and lipids. If that was the case then it might be possible that these studies captured only one of the two functions. Recently, two independent studies showed that TMEM16F is a dual function channel/scramblase [31,30]. They showed that TMEM16F elicited Ca^{2+}-dependent phospholipid scrambling coinciding with non-selective ionic currents. They proposed that ions leak through the lipid pathway during bi-directional lipid transport. The main difference between these two studies is related to the ion and lipid pathway. While Yu and colleagues proposed that ions and lipids share a common pathway, with ionic conductance

being a consequence of lipid scrambling[31], Scudieri and colleagues found a corresponding TMEM16A pore mutation in TMEM16F that abolished channel but not scrambling activity, thus suggesting the two pathways are separated[30]. Therefore, according to these results it seems that TMEM16F is a dual function channel/scramblase, although it is not clear how lipids and ions are transported and why some TMEM16 members seem to be only channels or scramblases.

2.2.4 Other TMEM16s: phospholipid scramblases and more

Very little is known about the other TMEM16 members. Some TMEM16s seem to be solely phospholipid scramblases[32]. By expressing TMEM16 C, D, G and J (in addition to F) in TMEM16F$^{-/-}$ mouse lymphocytes and measuring, Suzuki and colleagues showed that all these TMEM16 members elicited phospholipid scrambling, although the specificity for substrates varied between homologues. Furthermore, they showed that these TMEM16s failed to give rise to Ca^{2+}-activated Cl- currents in HEK 293T cells, as previously shown[90]. In addition to its putative scrambling function, TMEM16C was shown to facilitate Na^{+}-activated K^{+} currents by SLACK channels in rat sensory neurons and regulate pain processing[50]. Subdued, from *Drosophila melanogaster*, was shown to be a CaCC, providing evidence for conserved biophysical properties of some TMEM16 channels throughout evolution, and involved in thermal nociception[91]. Ist2 from *Saccharomyces cerevisae* acts as a tethering protein, in conjunction with other proteins, connecting the cortical endoplasmic reticulum and the plasma membrane[92,93]. We showed, by over-expressing, purifying and

reconstituting it that Ist2 does not mediate Ca^{2+}-dependent phospholipid scrambling (*see Chapter 3.1.4*). Overall, the TMEM16 family is characterized by a high degree of functional divergence. It will be interesting to understand if these different functions are underlined by the same functional framework or if there are some major structural differences among different TMEM16 proteins.

2.3. afTMEM16 is a dual function channel/scramblase

We sought to solve the controversy surrounding the role of TMEM16 proteins in phospholipid scrambling and whether they are phospholipid scramblases or channels regulating unknown scramblases by over-expressing, purifying and functionally reconstituting TMEM16 proteins. The first part of my thesis will focus on the functional characterization of afTMEM16, a fungal homologue from *Aspergillus fumigatus*. We found that afTMEM16 is a Ca^{2+}-dependent dual function channel/scramblases. This was the first direct proof that the TMEM16 family comprises phospholipid scramblases, helping resolve the controversy regarding their functional role and showing that TMEM16 proteins can act as ion channels and scramblases at the same time. Importantly, this is not a general property of the family, as we showed that purified TMEM16A and Ist2 do not show any scrambling activity. We found that, as previously shown for TMEM16A, B and F, a highly conserved Ca^{2+}-binding region modulates afTMEM16 activity, suggesting that besides the different functions TMEM16 proteins share a similar Ca^{2+} modulation. In afTMEM16 it regulates both channel and scrambling activity, posing the questions of whether also the substrates

share the same pathway and whether TMEM16 proteins share a similar structural framework or have evolved from ancestral dual function proteins into channels and scramblases as a consequence of a structural rearrangements.

2.4. nhTMEM16: X-ray crystal structure of a TMEM16 Ca^{2+}-dependent phospholipid scramblase

An important breakthrough in our understanding of the TMEM16 family came in 2015 when Brunner and colleagues solved the crystal structure of a TMEM16 phospholipid scramblase[33]. The structure of nhTMEM16, from the fungus *Nectria haematococca,* was solved at 3.3 Å in the presence of Ca^{2+}. nhTMEM16 is 48% identical to afTMEM16, with >70% homology within the transmembrane regions (**Figure 4**). The authors showed, by reconstituting nhTMEM16 in proteo-liposomes, that it is a Ca^{2+}-dependent phospholipid scramblase with biophysical properties almost identical to afTMEM16. nhTMEM16 scrambles different types of lipids in the presence of Ca^{2+} and less but substantial activity was observed when Ca^{2+} was chelated by EGTA. Interestingly, unlike afTMEM16, no currents generated by nhTMEM16 could be detected in planar lipid bi-layers or with patch-clamp recording of HEK 293T cells.

nhTMEM16 is comprised by ten transmembrane segments, preceded by two short α-helixes forming an amphiphilic hairpin. It is a homodimer with a twofold symmetry (**Figure 4A**), in agreement with previous findings showing that TMEM16 proteins form dimers [94,95]. A large pore-like structure, called the dimer

cavity, is observed across the transmembrane region. It contains two separate entrances, 15 Å wide, at the extracellular side which merge into a large vestibule, ~30 Å wide, at the intracellular half of the membrane. This vestibule, which is also directly exposed to the membrane, is made by highly conserved hydrophobic and aromatic residues while the two separate entrances are made by charged and polar residues. They were not able to assign any functional relevance to it.

The most remarkable feature of the structure is the subunit cavity: each monomer forms a cavity 8-11 Å wide that is directly exposed to the membrane, is present (**Figure 4A**). Helices 4 and 6 delimit the cavity with helix 5 lining the back of it. The inside of the cavity is hydrophilic and interestingly some of the corresponding mutations that alter ion selectivity in TMEM16A are located in this cavity. These features make the cavity the prime candidate for the translocation pathways for both ions and lipids. Indeed, the authors propose a lipid translocation mechanism where the head group of a phospholipid would make contact with residues within the cavity and this would allow lipid translocation in a bi-directional, semicircular fashion (**Figure 4B**).

The Ca^{2+}-binding site is formed by residues located in helices 6-7-8, within the membrane, right behind the lipid pathway. The structure shows two Ca^{2+} ions bound per monomer. It was shown that Ca^{2+} sensitivity of TMEM16A, B and F is voltage-dependent: at positive voltages the affinity is higher than at negative voltages[25,27,77,78,96]. The location of the Ca^{2+}-binding region, buried within the membrane, explains these results. Remarkably, experiments performed on

TMEM16A, TMEM16F and afTMEM6 correctly identified this region. The Ca^{2+}-binding site is comprised by six, highly conserved residues: three glutamates (E506, E535 and E452), two aspartates (D503 and D539) and one asparagine (N448) (**Figure 4C**). These residues are highly conserved in all TMEM16s and in fact were already shown to be crucial for Ca^{2+}-sensitivity in TMEM16A and F[75,77], supporting the hypothesis that the Ca^{2+}- sensitivity of the TMEM16 family is underlined by the same mechanism.

From the structure it is not clear where the ion pathway is located. The observation that point mutations altering ion conduction in TMEM16A and F are located along the cavity suggests that ions and lipids would go through the same pathway. This would be in agreement with the hypothesis that ions leak through the lipid pathway as a consequence of lipid scrambling in TMEM16F[31,97]. If this was the case, it is not clear what residues would line the pore and confer ion selectivity to TMEM16 channels and why TMEM16A and B (CaCCs) do not translocate lipids. Another possibility, although unlikely in light of mutagenesis results that showed it is possible to confer scrambling activity to TMEM16A by swapping 15 residues from TMEM16F[31], is that channels and scramblases do not share a similar structural framework, as proposed by Brunner and colleagues[33]. This would explain why some of the mutations found to alter ion conductance in TMEM16A and F are not located within the cavity but far away in extracellular loops[25].

Finally, it is worth noting that while Brunner and colleagues claimed, based on electrophysiological recordings, that nhTMEM16 is not an ion channel,

our group has convincing evidence that, similar to afTMEM16, nhTMEM16 is a Ca^{2+}-dependent dual function channel/scramblase. While these experiments are not shown as I was not directly involved and because it is still a work in progress, it is important in the context of the family and to understand the structural basis for the differences between TMEM16 channels, scramblases and dual function proteins.

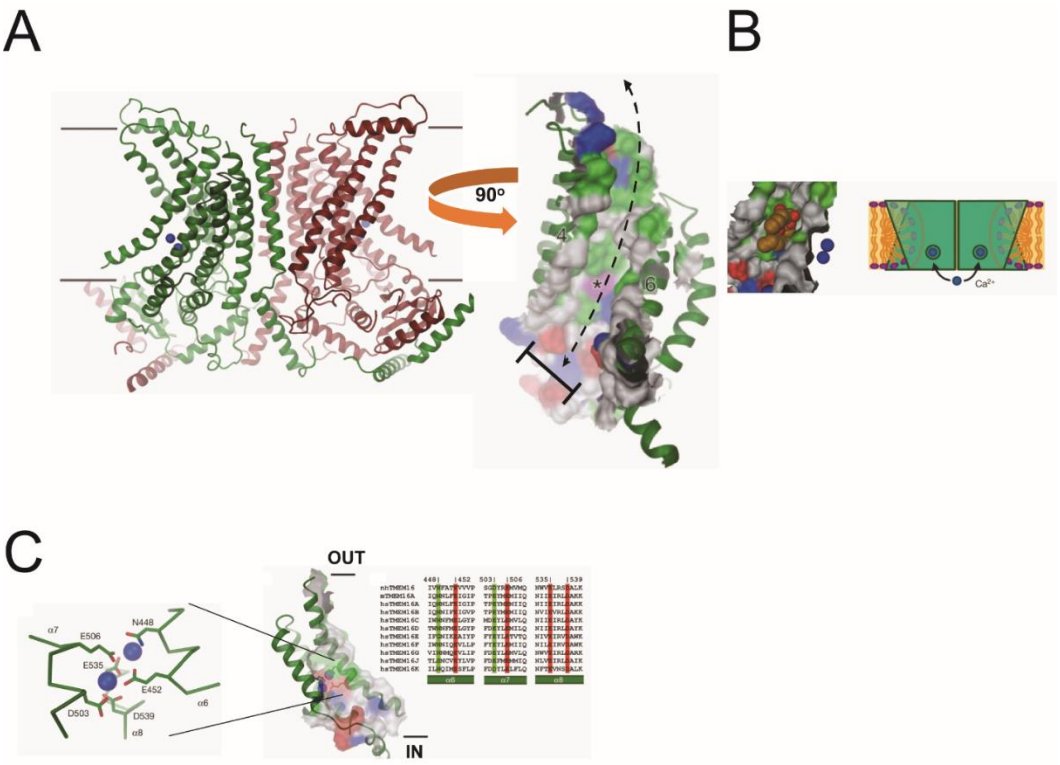

Figure 4: crystal structure of nhTMEM16.
A: Crystal structure of a TMEM16 family member from the fungus *Nectria haematococca* that operates as a Ca^{2+}-activated phospholipid scramblase[33]. Each subunit of the homodimeric protein contains ten transmembrane helices and a hydrophilic membrane-traversing cavity, 8~11 Å wide, exposed to the lipid bilayer, proposed to act as the lipid pathway. Two Ca^{2+} ions (blue spheres) are found in each monomer. **B**: Proposed phospholipid scrambling mechanism. Lipid translocation occurs via phospholipid head group-cavity forming residues (a model of phosphatidylcholine in the subunit cavity is shown). **C**: The Ca^{2+}-binding site (view from within the cavity), comprised by six residues in TM6-7-8). Conserved amino acid are highlighted (red: identical, green: homologous)

2.5. Investigating the mechanisms underlying lipid scrambling and Ca^{2+}-modulation in afTMEM16

The structure of nhTMEM16 signed a major shift in our work. With a structure of a TMEM16 scramblase we started to compare the results we and others obtained and the structural features of nhTMEM16. Furthermore, the proposed lipid scrambling mechanism, based on headgroup-cavity interactions within the ~1nm wide lipid pathway, provided us with new models and questions. The second part of the thesis is influenced by the nhTMEM16 structure and will focus on our investigation of the lipid scrambling mechanism and how Ca^{2+} modulates the process. We investigated how the size of the phospholipid headgroup would influences phospholipid scrambling. We found that tight interactions within the lipid cavity might not be required for scrambling to occur as head groups as large as 5 nm in diameter are translocated in a similar manner to standard phospholipids with head groups of ~0.5 nm. We also found that scrambling is slowed but not abolished when the headgroup size is increased in the apo state, suggesting the presence of two distinct open states in the presence or absence of
Ca^{2+}.

3. Results

This section is divided in two major parts. The first part (3.1) addresses the question of whether TMEM16 proteins are phospholipid scramblases. We aimed to over-express and purify TMEM16 homologues in order to reconstitute them into artificial vesicles to directly test scrambling activity and found that afTMEM16 is a dual function, Ca^{2+}-dependent channel/scramblase. This part focuses on the functional characterization of afTMEM16 and the results described were published in 2013[98]. The second part (3.2) aims to investigate the mechanisms underlying phospholipid scrambling and its Ca^{2+} modulation and it is driven by the structure of nhTMEM16[33] and the mechanism of scrambling proposed based on it. We investigated how the size of the phospholipid head groups influences phospholipid scrambling in the Ca^{2+}-bound and apo states. We found that, while in the presence of Ca^{2+} increasing the size does not influence the ability of afTMEM16 to scramble lipids, in the apo state scrambling is progressively reduced, but not abolished. This led us to propose a model where there are two distinct conductive states in the presence and absence of Ca^{2+}, and Ca^{2+} is widening the pathway. A manuscript focused on the results described in this second part is currently being prepared.

3.1. afTMEM16 is a Ca^{2+}-gated channel and a Ca^{2+}-dependent phospholipid scramblase

3.1.1. Over-expression, purification and functional reconstitution of afTMEM16

We screened for TMEM16 homologues suitable for over-expression and purification in order to purify TMEM16 proteins and reconstitute them into artificial membranes. Among all the candidates we found that a fungal homologue for *Aspergillus fumigatus* (AFUA_4G02970 - *Aqy1*, PubMed gene ID: 3504033) gave us the best results in terms of expression, yield after detergent purification and stability. We renamed the protein afTMEM16. Among mammalian proteins the relationship is closest to TMEM16H and K (**Figure 3**). The protein runs as a monodisperse peak on a size-exclusion chromatography column (**Figure 5A**) and as a single band on SDS-PAGE gel (**Figure 5B**). Unless otherwise stated afTMEM16 was reconstituted in E. coli polar extract or E. coli polar:Egg PC (60%) (3:1) lipids.

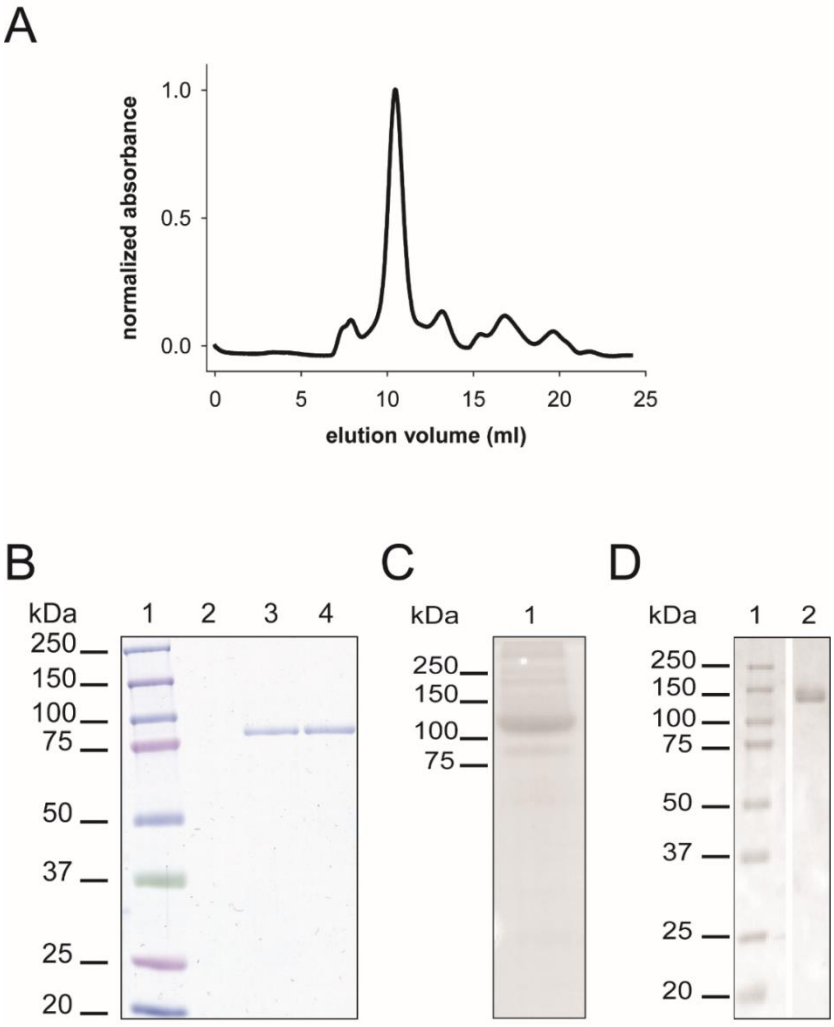

Figure 5: purification of afTMEM16.
A: afTMEM16 was solubilized in digitonin and purified on a Superdex 200 column. **B**: purified afTMEM16 was loaded on SDS-PAGE gel and stained with Coomassie Brilliant Blue. *Lane*: 1: Marker; 2: purified product from vector-only transformed cells; purified afTMEM16; 4: purified D511A/E514A mutant. **C**: hTMEM16A. **D**: Ist2p. The predicted MW for the proteins are afTMEM16 = 85kDa; hTMEM16A = 114kDa; Ist2p = 105kDa.

3.1.2. afTMEM16 is a Ca^{2+}-gated ion channel

The first question we addressed was whether afTMEM16, like TMEM16A and B, was a Ca^{2+}-activated ion channel. We performed single channel measurements with afTMEM16 reconstituted in proteo-liposomes (**Figure 6A**). After fusing these vesicles to pre-formed planar lipid bilayers made by POPE:POPG (3:1) we observed single channels of high conductance, ~300 pS (n=7) (**Figure 6B, D**). The channels were poorly selective; their currents reversed at ~-9 mV in the presence of a 10-fold KCl gradient, indicating a minor cationic preference of P_{K^+}/P_{Cl^-}~1.5 (**Figure 6D**). The channels were gated by both voltage and Ca^{2+}: the open probability increased at depolarizing potentials, reaching ~1 at V>-50 mV and removing Ca^{2+} from the *Cis* chamber reduced channel activity at -100 Mv (**Figure 6E-H**). No channels were detected in 35 recordings where liposomes reconstituted with mock preparations were fused to the bilayers, giving us confidence that the currents detected were indeed due to the presence of afTMEM16 (**Table 1**). Although we were able to observe ionic currents by afTMEM16, the rate of success was low, ~3%, and the currents quickly disappeared (duration ~ 300s) (**Table 1**). We reasoned that this might be due to the bilayer lipid composition causing the protein to become inactive after the initial vesicle fusion events, as the lipid forming the proteo-liposomes would diffuse into the bi-layer and the proteins would quickly become surrounded by those lipids. Thus we tried to change the bi-layer lipid composition to E.Coli:Egg PC (3:1), which is the lipid composition of the proteo-liposomes, and indeed the rate of success increased to ~11%. Unfortunately, likely due to the nature of the

mixture (extract and not synthetic) the bi-layers were not stable ad collapsed shortly after they were formed, resulting in an even shorter duration of channel activity (**Table 1**).

Given the issues with the planar lipid bi-layer recordings we decided to exploit the poor ion selectivity of afTMEM16 detected by single channel recordings to develop a “flux” assay for its ion channel activity. Liposomes containing 1 or more open afTMEM16 channels should not maintain a KCl gradient when exposed to a low KCl solution while protein-free liposomes (or those with closed channels) should. Therefore, the Cl^- content of liposomes exposed to a large KCl gradient is a direct measure of the channel activity of afTMEM16 (**Figure 7A**). Indeed, when afTMEM16-containing liposomes, loaded with high KCl content (300mM), are passed through a buffer exchange column (G-50 beads) equilibrated in 1 mM KCl, they lose almost all the KCl content in the presence of symmetrical Ca^{2+}, as shown by measuring the Cl^- amount left upon addition of detergent to solubilize the liposomes and release their content (**Figure 7B-C**). Compared to protein-free liposomes which, as expected, retain their KCl content, afTMEM16-containing liposomes lose ~ 80% of KCl during the buffer exchange step. Consistent with the single channel measurements, this is a Ca^{2+}-dependent process as afTMEM16-containing liposomes retain almost all the KCl content (~75%) in the presence of symmetrical EGTA. Importantly, when the lipid composition of the liposomes was changed to POPE:POPG (3:1), the same composition used to form planar lipid bilayers, afTMEM16 channel activity

is severely reduced (**Figure 7C**), consistent with the observation of rare, short-living single channels detected (**Table 1**).

Finally, we tested whether large ions would permeate through the channel. We found that TEA^+ is permeable while $NMDG^+$ is not (**Figure 7C**). Given that TEA^+ has a radius of ~ 4 Å and $NMDG^+$ of ~ 6.5 Å, the narrowest part of the pore should be between those values. In conclusion, these experiments show that afTMEM16 is a Ca^{2+}-gated, poorly selective ion channel of large conductance with voltage dependence.

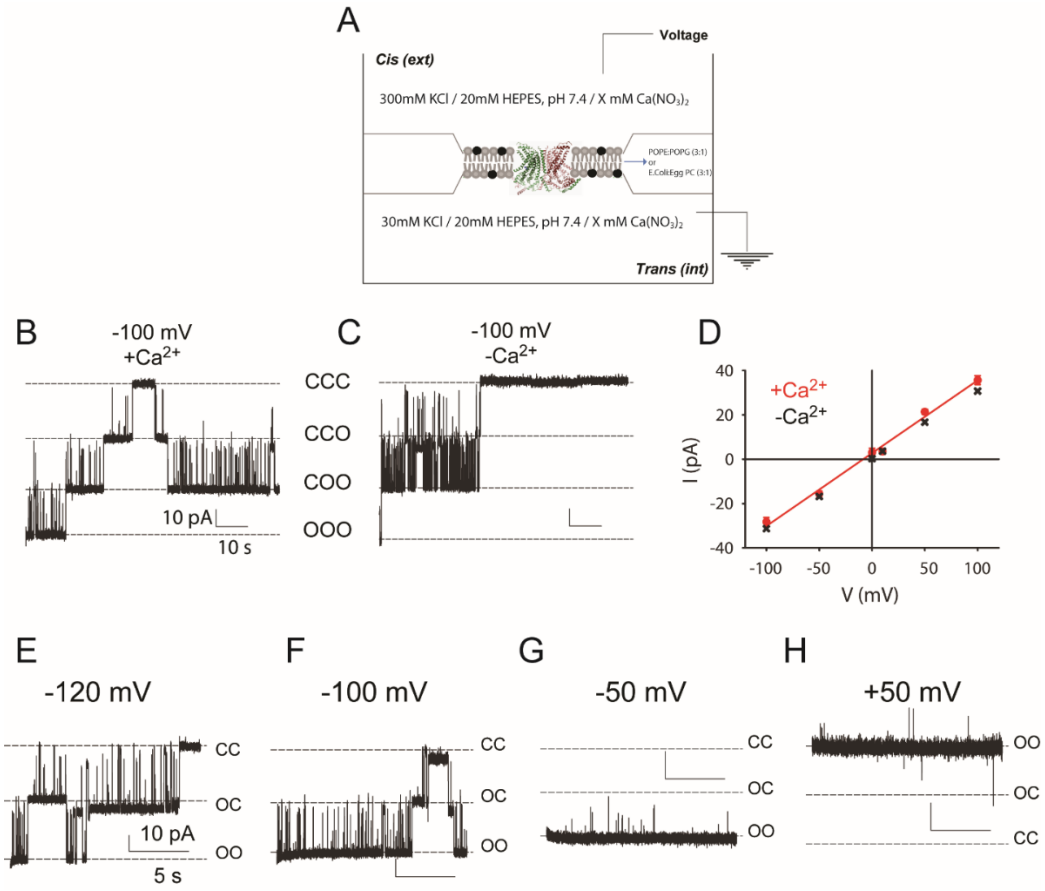

Figure 6: afTMEM16 is a Ca^{2+}-gated, voltage dependent ion channel.
A: schematic of the horizontal planar lipid bi-layer setup. **B-C:** Recording of 3 afTMEM16 channels at -100 mV with 0.5 mM Ca^{2+} (B) or 1 mM EDTA on the Cis side (C). **D:** Current-Voltage plot of afTMEM16 in the presence of a 10-fold KCl gradient with (red squares) or without (black crosses) Ca^{2+}. Red line: linear fit with V_{rev}= -8.3 ± 2.7 mV. **E-H**: Recordings from a bilayer containing 2 independent afTMEM16 channels at -120 mV (E), -100 mV (F), -50 mV (V) and +50 mV (H). Open (O) and closed (C) states are indicated by dashed lines (B-H).

Table 1: statistics for bi-layer recordings.
Bi-layers formed in POPE:POPG (3:1) were stable (>10 min on average). All the experiments were channels were observed (n=7) were performed in the presence of 0.5 mM Ca^{2+}, in n=2 of those experiments the Cis chamber was perfused with a solution containing 1mM EDTA to remove Ca^{2+}. In E. Coli: Egg PC (3:1) the bi-layers were extremely unstable (<5 min on average) preventing recordings of afTMEM16 channels.

Lipid	Protein	Total number of experiments	Number of experiments with channels	% of successful experiments	Average recording duration (s)	Wait time (min)
POPE:POPG (3:1)	**afTMEM16**	263	7	2.7	280 ± 110	>10
	Mock	35	0	0	0	>10
***E. Coli* : Egg PC (3:1)**	**afTMEM16**	18	2	11.1	20 (exp#1) 80 (exp#2)	< 5

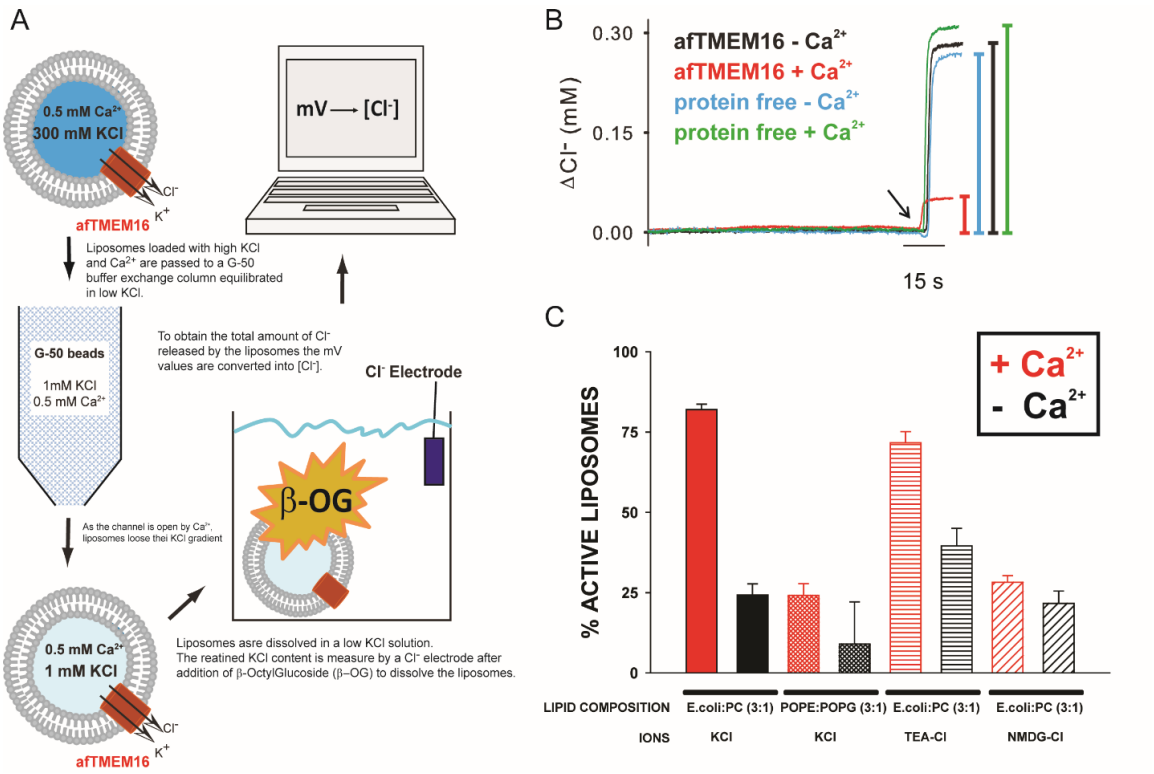

Figure 7: Cl^- flux assay.
A: Schematic of the assay. Liposomes loaded with 300 mM KCl are passed through a G-50 column equilibrated in 1 mM KCl to exchange the buffer. In the presence of Ca^{2+}, afTMEM16 channel is open and the KCl gradient is lost during this step. In the presence of EGTA afTMEM16 channel is closed and the proteo-liposomes retain their KCl gradient. Liposomes are dissolved in a solution containing 1 mM KCl and the amount of KCl retained by the liposomes is measured by a Cl^- electrode upon addition of β-Octylglucoside (β-OG) to solubilize the liposomes. **B**: Measure of Cl^- content in protein-free liposomes in 0.5 (green) or 0 (blue) mM Ca^{2+} and in afTMEM16-containing liposomes with 0.5 (red) or 0 (black) mM Ca^{2+}. Liposomes were prepared in E. coli Polar : Egg PC (3:1). Arrow denotes the addition of detergent. Vertical bars represent the value of ΔCl^-. **C:** Fraction of trapped Cl^- represented as % of active liposomes normalized to each protein-free condition. Proteoliposomes reconstituted in E. Coli Polar : Egg PC (3:1) or POPE:POPG (3:1) with (red) or without (black) 0.5 mM Ca^{2+} and with K^+, TEA^+ or $NMDG^+$. The experiments were repeated at least three times, Error bars are the s.e.m.

3.1.3. afTMEM16 is a Ca^{2+}-dependent phospholipid scramblase.

The main question we wanted to answer in a definitive manner was whether afTMEM16 was a phospholipid scramblase. To assay scrambling we reconstituted afTMEM16 into liposomes containing trace amounts (0.5 mole %) of phospholipids bearing a nitrobenzoxadiazole (NBD) fluorophore and measured the time course of fluorescence loss due to the addition of the membrane-impermeant sodium dithionite[99, 11]. In protein-free liposomes the fluorescence decay is expected to reach 50%, as the NBD-phospholipids equally distribute between the two leaflets and the only outer-leaflet NBD-phospholipids are reduced. In scramblase containing liposomes, the extent of fluorescence loss is expected to reach 100%, as NBD-lipids are translocated from the inner to the outer leaflet (**Figure 8A**). As expected, the fluorescence loss of phosphatidylethanolamine (NBD-PE) upon dithionite addition in protein-free liposome is ~50% with a decay of fluorescence well described by a single exponential function with time constant ~20s, regardless of the presence of Ca^{2+} in solution (**Figure 8B**). In proteo-liposomes reconstituted with high copy numbers of afTMEM16 (5 mg /mg of lipids) in the presence of saturating Ca^{2+} (0.5 mM) we observed ~85% fluorescence reduction (**Figure 8B**). This suggests that afTMEM16 is a phospholipid scramblase. Importantly, Ca^{2+} modulated the rate of lipid scrambling. In high Ca^{2+} the fluorescence decay reached a plateau in ~100 s after the addition of dithionite while removal of Ca^{2+} by EGTA slowed the process so that steady state was not reached after 900 s. This is reflected in the appearance of a second kinetic component in the fluorescence decay time

course, with time constant of ~400s (**Figure 8B**). The two components in the fluorescence decay do not reflect two distinct processes mediated by afTMEM16, rather they are a complex function of the rates of scrambling and dithionite reduction. At low Ca^{2+} the two components are sufficiently different that we can assign the fast one to the dithionite reduction of the outer leaflet and the slow one to the progressive exposure of inner-leaflet lipids to the outside. In contrast, at high Ca^{2+} the fluorescence decay is well described by a single exponential function with a time constant similar to that seen in protein-free liposomes. Therefore, at high Ca^{2+} the fluorescence decay is rate limited by the chemical reduction of the NBD fluorophore by dithionite rather than by lipid scrambling. If we assume that an average liposome contains ~10^6 lipids[100] and ~5 copies of purified afTMEM16 (*see chapter 3.1.5*) then we can estimate that the rate of lipid flipping in 0 Ca^{2+} is ~400 lipid s^{-1} and that in saturating Ca^{2+} it is >10^4 lipid s^{-1}, a >20-fold increase in rate (*see methods*).

The Ca^{2+}-dependence of rate of lipid scrambling is readily visualized by measuring the fluorescence decay in liposomes prepared in symmetrical 0 Ca^{2+} and to which, ~60 s after the addition dithionite, 0.5 mM Ca^{2+} was added to the extraliposomal solution (**Figure 8C**). The sudden increase in Ca^{2+}_{ex} "turns on" the scramblases with extracellular ligand binding site and the rate of fluorescence decay increases ~20-fold. A comparable increase in rate was visible upon adding 1 µM Ca^{2+}_{ex} and 10 µM Ca^{2+}_{ex} suggesting that afTMEM16 has a micromolar Ca^{2+} sensitivity. These results suggest that afTMEM16 is a phospholipid scramblase and that Ca^{2+} modulates its scrambling rate by more than 20-fold.

As we showed that afTMEM16 is an ion channel we needed to rule out the possibility that the fluorescence decay reflected dithionite permeation through afTMEM16 rather than phospholipid scrambling. We prepared liposomes in the presence of 60 mM NBD-Glucose, removed the external NBD-Glucose via spin column and monitored the time course of fluorescence decay after dithionite addition. If dithionite permeates through afTMEM16 it will gain access to the NBD-Glucose trapped inside the vesicles and reduce the fluorophore. In this case, we expect to see a >80% drop in fluorescence with kinetics similar to those seen for scrambling in the presence of 0.5 mM Ca^{2+} (**Figure 8D**). In contrast, if dithionite does not permeate through afTMEM16 then the total fluorescence should remain nearly constant. This is the case: in afTMEM16 proteo-liposomes the fluorescence decays very slowly and at a rate that is nearly indistinguishable from that seen in protein-free liposomes ~0.02% of total fluorescence per second in both cases (**Figure 8D**). The initial jump immediately following the addition of dithionite reflects the incomplete removal of NBD-Glucose from the extraliposomal solution by the buffer exchange column. This shows that we are indeed monitoring phospholipid scrambling by afTMEM16 and not dithionite influx through the channel.

Finally, to rule out the possibility that scrambling mediated by afTMEM16 might be a process specific to the modified reporter lipids, in which one fatty acid chain has been replaced with a short chain bearing an NBD fluorophore, we examined the dependence of the rate of fluorescence decay on the concentration of NBD-PE. If afTMEM16 specifically transports only NBD-labeled lipids then the

time constant of fluorescence decay should depend strongly on the concentration of NBD-PE. If, on the other hand, all the lipids in a liposome are scrambled by afTMEM16 then the kinetics should be independent from the NBD-PE concentration. These measurements were performed in 0 Ca^{2+}, a regime where the rate of lipid scrambling is ~ 20-fold slower than the rate of dithionite reduction of the NBD-fluorophore so that the two processes can be readily separated. We found that upon changing the NBD-PE concentration 100-fold (from 0.05 to 5 mole %) the time constants of fast and slow decay are nearly unaffected (**Figure 8E**) indicating that afTMEM16 does not specifically transport only NBD-labeled lipids, but rather that it scrambles all the lipids contained in each vesicle.

To further strengthen our conclusion that afTMEM16 is a phospholipid scramblase, we used fatty-acid free bovine serum albumin (BSA) as a topological probe of scrambling. BSA extracts NBD-phospholipids and quenches their fluorescence by ~50% [11 101] (**Figure 8F**). Consistent with expectations, we saw ~27% fluorescence reduction upon BSA addition to protein-free liposomes and ~53% reduction in afTMEM16-containing liposomes with Ca^{2+}-dependent kinetics (**Figure 8F**). Therefore, the dithionite- and BSA-based assays independently demonstrate that afTMEM16 is a Ca^{2+}-dependent phospholipid scramblase.

We then tested the lipid selectivity of afTMEM16. As phospholipid scramblases show poor lipid selectivity [10,12], being able to move lipids with different sizes and charges, we tested several NBD-labelled lipids in addition to NBD-PE. We found that, indeed, afTMEM16 is able to scramble lipids with different properties. Phosphatidylserine (PS), phosphatidycholine (PC), PE with

the NBD group attached to the headgroup rather than the acyl chain (N-NBD-DPPE), glucosylceramide and the cation lipid DOTAP are all scrambled by afTMEM16 (**Figure 8H, J**). While some lipids display slightly differences in the kinetics of scrambling, these results show that afTMEM16 is non selective for lipids, as expected from a phospholipid scramblase.

It is important to note that the incomplete loss of fluorescence suggests that a small fraction of vesicles are refractory to protein insertion, as previously reported[11,100,102]. We found that among all tested reconstitution conditions the value of the refractory pool varies a minimum value of ~5%, to a maximum value of ~30%. This is consistent with the notion that liposome size and shape are affected by the composition of the buffer and of the lipid membrane[103,104]. This refractory pool might reflect the amount of liposomes that somehow during the process of forming the unilamellar vesicles by extrusion do not get any protein incorporated or it might reflect the presence of some small liposomes trapped inside bigger ones. This would be consistent with the observation that the fluorescence signal drops to 0 after addition of detergent to solubilize the liposomes. Importantly, these numbers match what we observed for the flux assay, corroborating the idea that this refractory fraction of liposomes is likely due to the process of forming the vesicle rather than being specific to the protein or the assay.

.

Figure 8: afTMEM16 is a Ca^{2+}-dependent phospholipid scramblase.
A: Dithionite-based scramblase assay. NBD- lipids (red) are irreversibly reduced (black) by dithionite. In protein-free liposomes only the outer-leaflet fluorophores are reduced. **B**: Fluorescence loss of NBD-PE: protein-free liposomes with 0.5 mM Ca^{2+} (green); afTMEM16 proteoliposomes with 0.5 mM Ca^{2+} (red) or in 0 Ca^{2+} (black). **C**: Scrambling in symmetrical 0.5 mM Ca^{2+} (red) or 0 mM Ca^{2+} (black). The blue trace corresponds to an experiment started in symmetrical 0 mM Ca^{2+}, and at t~160 s, 0.5 mM) Ca^{2+}_{ex} is added to the extraliposomal solution. Dithionite was added at *t*=100 s in all cases and is not shown. For clarity, only the F/F_{max} interval between 0.15 and 0.45 is shown. **D**: Dithionite does not permeate through afTMEM16. Left panel: schematic representation of the NBD-Glucose accessibility experiments. Right panel: replicate time courses of the NBD-Glucose fluorescence decay in protein-free liposomes (green) and afTMEM-containing liposomes in the presence of 0.5 mM Ca^{2+}. Fits are shown in blue (protein-free) and black (afTMEM16). Dashed grey line represents phospholipid scrambling by afTMEM16. **E**: Scrambling is not specific for NBD-lipids. Left panel: time course of fluorescence decay in afTMEM16 in the presence of 0.05 (green), 0.5 (black) and 5 (red) mole % NBD-PE. All the experiments were performed in 0 mM Ca^{2+}. Right panel: time constants of fluorescence decay for protein-free liposomes (τ_0) and afTMEM16-containing liposomes (τ_{fast} and τ_{slow}). **F**: Scrambling measured with BSA. Left panel: schematic representation of the assay. Right panel: Representative traces of the time course of fluorescence loss after addition of BSA (*) in protein-free (green) and afTMEM16-containing liposomes (red: 0.5 mM Ca^{2+}; black: 0 mM Ca^{2+}). **G**: Not all TMEM16s are scramblases. Fluorescence loss in liposomes reconstituted with CLC-ec1 (blue), hTMEM16A (solid lines) or Ist2p (dashed lines) in the presence (red) or absence (black) of Ca^{2+}. **H**: Lipid selectivity of afTMEM16. Time course of fluorescence loss in liposomes containing NBD-phosphatidylserine (PS), NBD-head labelled phosphatidylethanolamine (DPPE), NBD-phosphatidylcholine (PC), NBD-Glucosylceramide (GC) and NBD-DOTAP in the presence (red) and absence (black) of Ca^{2+}. Protein-free liposomes are in green. **I**: Quantification of scrambling activity. Fluorescence values at t=60s (vertical dashed line), when the outer leaflet is completely reduced, are measured. The difference between the protein-free liposomes and the afTMEM16-containing liposomes is ΔF, which is then normalized to the ΔF of NBD-PE to obtain the % of activity. **J**: Percentage of scrambling activity for each NBD-lipid. In all experiments, unless otherwise noted, * denotes addition of dithionite at t=100s. Experiments were repeated at least three times. Error bars are the s.e.m

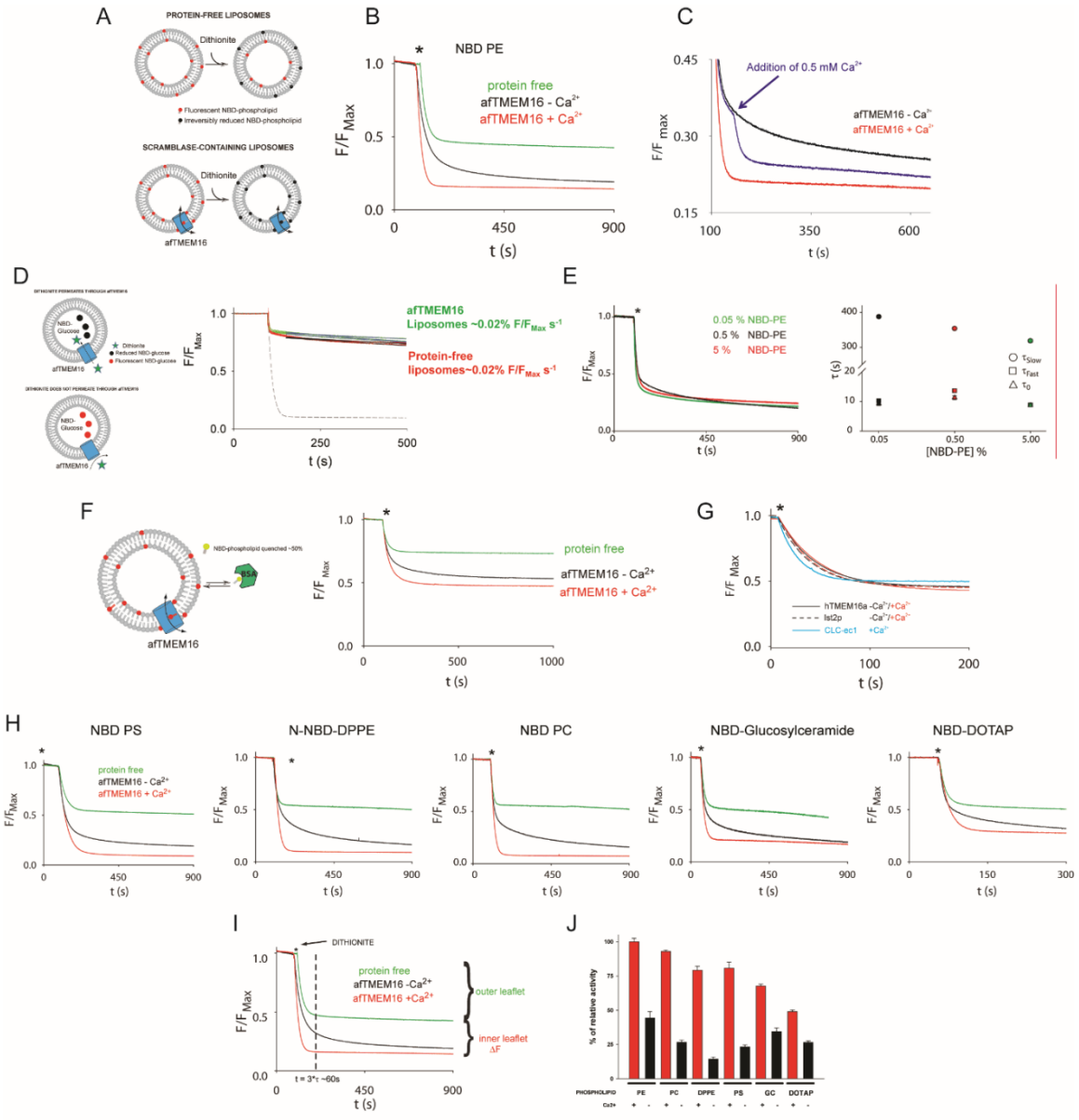
A
PROTEIN-FREE LIPOSOMES
Dithionite
Fluorescent NBD-phospholipid
Irreversibly reduced NBD-phospholipid
SCRAMBLASE-CONTAINING LIPOSOMES
Dithionite
afTMEM16
B
NBD PE
protein free
afTMEM16 - Ca2+
afTMEM16 + Ca2+
F/FMax
t (s)
C
Addition of 0.5 mM Ca2+
afTMEM16 - Ca2+
afTMEM16 + Ca2+
F/F max
t (s)
D
afTMEM16
Liposomes ~0.02% F/FMax s-1
Protein-free
liposomes~0.02% F/FMax s-1
t (s)
E
0.05 % NBD-PE
0.5 % NBD-PE
5 % NBD-PE
t (s)
τ (s)
[NBD-PE] %
F
NBD-phospholipid quenched ~50%
BSA
afTMEM16
protein free
afTMEM16 - Ca2+
afTMEM16 + Ca2+
t (s)
G
hTMEM16a -Ca2+/+Ca2+
Ist2p -Ca2+/+Ca2+
CLC-ec1 +Ca2+
t (s)
H
NBD PS
N-NBD-DPPE
NBD PC
NBD-Glucosylceramide
NBD-DOTAP
protein free
afTMEM16 - Ca2+
afTMEM16 + Ca2+
t (s)
I
DITHIONITE
protein free
afTMEM16 -Ca2+
afTMEM16 +Ca2+
outer leaflet
inner leaflet
ΔF
t = 3*τ ~60s
t (s)
J
% of relative activity
PHOSPHOLIPID
PE
PC
DPPE
PS
GC
DOTAP
Ca2+

3.1.4. Not all TMEM16 homologues are phospholipid scramblases

We next tested whether lipid scrambling is a general property of all TMEM16 family members or if the presence of an integral membrane protein might disturb the lipid bilayer enough to induce scrambling. First, we verified that we do not detect lipid movement in proteo-liposomes containing CLC-ec1, a CLC-type H^+/Cl^- exchanger with no physiological connection to phospholipid scrambling, (**Figure 8G**). This is consistent with numerous previous reports showing that the mere presence of a membrane protein in vesicles does not promote rapid trans bilayer movement of lipids[11,105,106]. Then, we purified and reconstituted hTMEM16A, a CaCC with no link to phospholipid scrambling[25-27], and Ist2, a TMEM16 fungal homologue involved in membrane tethering[92,93], and found that neither protein mediates lipid scrambling regardless of the presence of Ca^{2+} (**Figure 8G**). Thus our data suggests that not all TMEM16 homologues are phospholipid scramblases.

3.1.5. afTMEM16 is a dual function channel/scramblase

To eliminate the possibility that either the channel or the scramblase activity is mediated by a co-purified contaminant rather than by afTMEM16 we examined the dependencies of these activities on the total protein reconstituted (**Figure 9**). If a channel and a scramblase are co-purified and present in different numbers, then the fractions of liposomes containing 0 copies of a protein, f_0, for the two activities should follow a Poisson distribution and diverge at low protein densities[11,102] (*see methods*). In contrast, if afTMEM16 is a dual function protein,

then the two fractions should co-vary. We determined f_0 at different protein concentrations using flux and scrambling assays and found that they co-vary (**Figure 9A**), with p_0 values of ~0.4 mg protein/mg lipid, indicating that both ion channel and lipid scrambling activities are mediated by afTMEM16. Our Poisson analysis also suggests that afTMEM16 assumes a dimeric architecture in the membrane. Predictions of the Poisson statistics for afTMEM16 as a monomer, dimer or tetramer based on experimental experiments from the flux, scrambling and BSA assays show that only when afTMEM16 is assumed to be a dimer the prediction correlates with the experimental data (**Figure 9C**). Therefore, as one afTMEM16 monomer is ~85 KDa, we can estimate that 5-6 dimers per liposome are reconstituted.

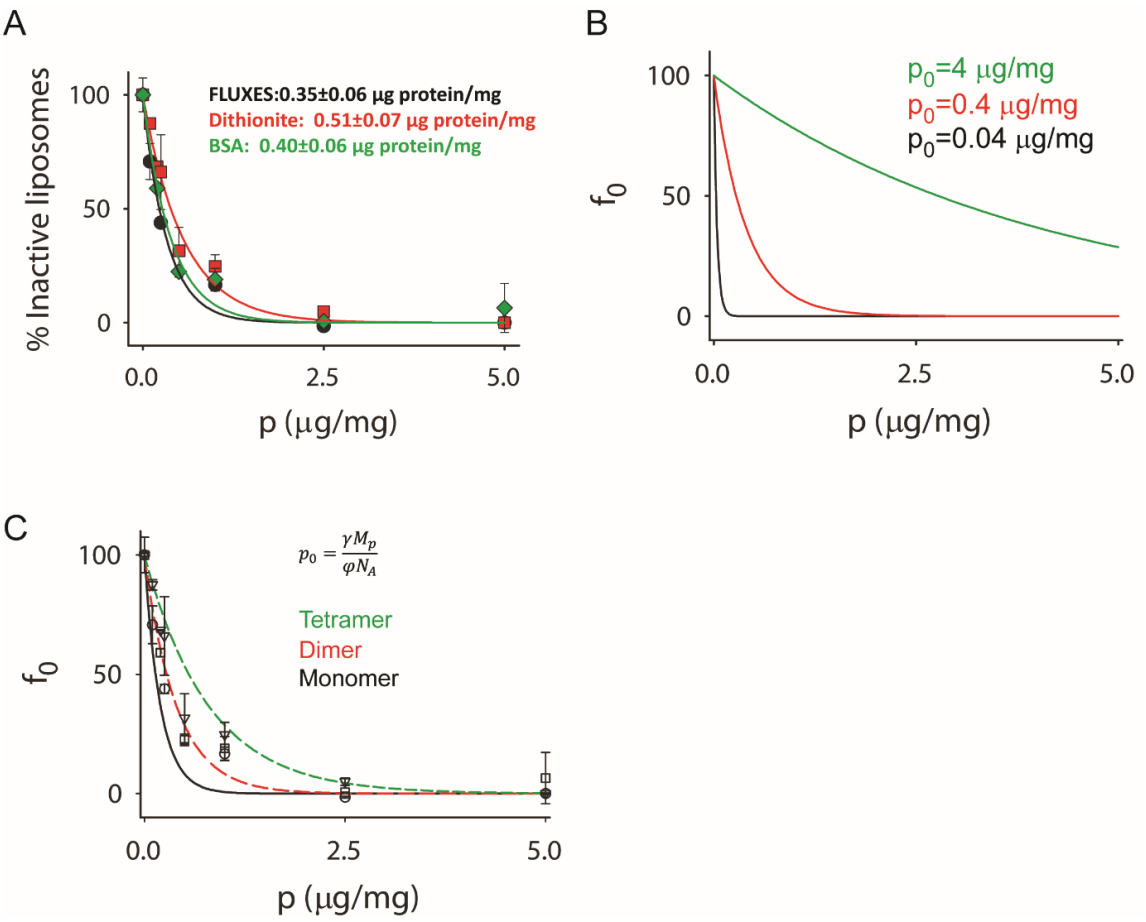

Figure 9: afTMEM16 is a dual function protein.
A: Dependence of ion channel and scrambling activities on protein concentration. Protein dependence of f_0^{norm} measured by flux (black) and lipid scrambling (dithionite (red) or BSA (green) assays. Solid lines are fits to $f_0^{norm}=e^{-p/p0}$ with p_0(Flux)= 0.35±0.06, p_0(Dithionite)= 0.51±0.07and p_0(BSA)= 0.40±0.06 μg protein/mg lipid. **B**: Simulated traces of f_0 for three different protein concentrations with p0 values of 0.04 (black), 0.4 (red) and 4 (green). **C**: Comparison of the predictions of the Poisson statistics for afTMEM16 as a monomer (black), dimer (red) and tetramer (green) woth experimental data derived from flux assay (circles) and scrambling assay (dithionite: squares; BSA: triangles). In all cases the data points represent an average of at least 3 independent experiments. Error bars are the s.e.m.

3.1.6. Comparison of afTMEM16 to mammalian TMEM16 channels

In addition to sensitivity to Ca^{2+} and voltage dependence, afTMEM16 channels share a number of properties with TMEM16A and TMEM16F. Our Poisson-dilution measurements (**Figure 9**) suggest that the functional afTMEM16 unit has a molecular mass of ~190 kDa, indicating that, like TMEM16A[94,95,107], afTMEM16 forms dimers in membranes. We found that afTMEM16 is a nearly non-selective ion channel (**Figure 6**), with P_{K^+}/P_{Cl^-} ~1.5. While this poor selectivity is unusual for better characterized channels[108], most TMEM16 ion channels appear to be poorly selective. For example, the anion/cation selectivity of TMEM16A is only ~0.15[25,27,75] and at least one of its splice variants has an even greater permeability to cations[109]. Similarly, cationic currents associated with TMEM16F also appear to be poorly selective, P_{K^+}/P_{Cl^-} ~7, and a point mutation decreases their selectivity to ~2.2[77], a value close to that of afTMEM16. Finally, the anionic currents associated with TMEM16F also display significant cation permeabilities, P_{Na^+}/P_{Cl^-}~0.3[87]. The afTMEM16 pore appears to be large. Our permeability experiments show that TEA^+ permeates through the channel while $NMDG^+$ appears to be excluded (**Figure 7C**) suggesting that the narrowest portion of the afTMEM16 pore is between 4-6.5 Å. Similarly, TMEM16A and 16F also allow the permeation of large ions such as $gluconate^-$ [109] and $NMDG^+$ [77] respectively, indicating that these other family homologues also have pores of wide diameters. Despite these similarities, we note that the single channel conductance of afTMEM16 is much higher than that of TMEM16A or 16F[25,77] and the channel remains open at negative voltages. The physiological implications of

the high conductance and poor selectivity of afTMEM16 are unclear, since we do not know its role in the physiology of its native organism, the pathogenic fungus *Aspergillus fumigatus*. Further work will be required to elucidate this point.

3.1.7. Similarities between afTMEM16 and mammalian scramblases

We found that afTMEM16 recapitulates the known properties of mammalian Ca^{2+}-dependent scramblases: Ca^{2+}-dependent, rapid and poorly selective lipid movement between membrane leaflets[10] (**Figure 8**). Removal of Ca^{2+} slows afTMEM16-mediated scrambling by >20-fold from $>10^4$ to ~400 lipid s^{-1}. Since we cannot determine the absolute rate of lipid scrambling in the presence of Ca^{2+}, to quantify the scrambling activity of afTMEM16 we measured the relative fluorescence (F) at t=60s (**Figure 8I**). As the time constant for protein free liposomes is 15-20s, this is equal to $3*\tau$ and all the outer leaflet has been reduced, therefore any F value below 0.5 represents phospholipid scrambling. We then normalize the values to the average F of the protein-free liposomes for each condition, which is ~0.5, as the baseline for zero percentage of activity and to the average ΔF of our standard condition, NBD-PE, in the presence of Ca^{2+} (**Figure 8I**). ΔF is the difference between F of protein-free liposomes and afTEM16 containing liposomes in NBD-PE $+Ca^{2+}$ and represents 100% of activity. We compare all the experiments to this value (**Figure 8J**). For example, in NBD-PE liposomes with no Ca^{2+} the relative activity is 44±4% compared to liposomes with NBD-PE in the presence of Ca^{2+}, indicating that while there is a significant reduction in activity, scrambling is still present.

We also found that afTMEM16 mediates the Ca^{2+}-dependent transport of a variety of lipids: NBD-PS, NBD-PE, and NBD-PC, as well as PE bearing the NBD fluorophore on the headgroup (N-NBD-DPPE), NBD-glucosylceramide and the cationic lipid DOTAP (**Figure 8H**). This is consistent with what was observed for native scramblase[10] . When compared to NBD-PE in the presence of Ca^{2+}, we found that the most well scrambled phospholipid is PC (~93% activity) followed by N-DPPE and PS (~80%), glucosylceramide (~70%) and DOTAP (~50%) (**Figure 8J**). While it seems that afTMEM16 is slightly selective for lipids, the differences in activity for some conditions in the presence of Ca^{2+} are due to different f_0 values, the population of liposomes that do not contain any protein (for example glucosylceramide), or to time constants slower than 20s which results in F values measured in a regime where scrambling is not completed (for example NBD-DOTAP).

3.1.8. A common Ca^{2+} binding site regulates ion and lipid transport in afTMEM16

We first characterized the Ca^{2+}-dependence of afTMEM16's channel and scramblase activities (**Figure 10**). The rate of afTMEM16-mediated lipid scrambling increased with Ca^{2+} (**Figure 10 A-D**), with a mid-point of activation of ~0.4 μM. Similarly, 0.5 μM Ca^{2+} was sufficient to open the afTMEM16 channel in flux assays (**Figure 10D**). The two activities share a similar selectivity for divalent cations: Ca^{2+} fully activates both transport functions, Mn^{2+}, Sr^{2+} and Ba^{2+} elicit intermediate responses, while Mg^{2+} and Cd^{2+} fail to activate either (**Figure 10 E-**

F). Thus both transport functions of afTMEM16 share the same apparent divalent selectivity of: Ca^{2+}>Mn^{2+}~Sr^{2+}>Ba^{2+}>Cd^{2+}~Mg^{2+}.

We then purified the afTMEM16 mutant D511A/E514A in which we charge-neutralized a conserved di-acidic motif that was shown to be critical for the Ca^{2+} sensitivity of TMEM16A and TMEM16F[75,77]. This mutant shows very minimal, Ca^{2+}-independent scrambling activity (**Figure 10G**), at lower rates than the wild-type protein in 0 Ca^{2+}. Similarly, liposomes reconstituted with the D511A/E514A mutant retained ~80% of their Cl^- content in 0.5 or 0 mM Ca^{2+}, indicating that this channel is not activated by Ca^{2+} (**Figure 10G**) Therefore, a single, evolutionarily conserved, Ca^{2+} binding site appears to regulate ion and lipid transport.

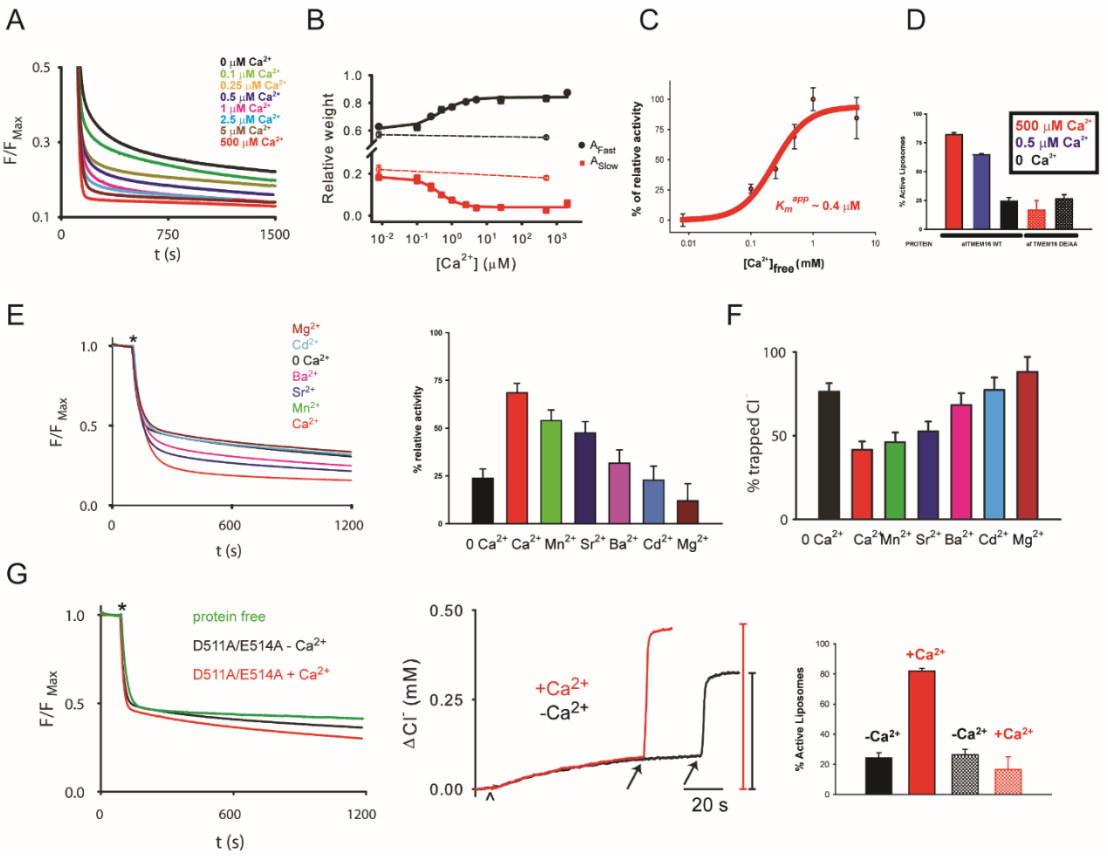

Figure 10: A common Ca^{2+}-binding site regulates ion and lipid transport in afTMEM16.

A: Phospholipid scrambling by afTMEM16 with 0 (black), 100 nM (green), 250 nM (mustard), 500 nM (blue), 1 μM (pink), 2.5 μM (cyan), 5 μM (brown) and 0.5 mM Ca^{2+} (red). **B:** Ca^{2+}-dependence of A_{Fast} (black circles) and A_{Slow} (red squares). Solid lines represent fits to a Hill equation with K_m^{App}(Fast)=0.44±0.13 μM, n(Fast)= 1.2±0.4 and K_m^{App}(Slow)= 0.44±0.07 μM, n(Slow)=1.5±0.3. WT afTMEM16: solid symbols and lines; D511A/E514A mutant: empty symbols and dashed lines. **C:** Ca^{2+}-dependence of phospholipid scrambling in afTMEM16 measured at t=60s. Values were normalized to the maximum and minimum to obtain % of activity. Fit to Hill equation. **D:** Ca^{2+}-dependence of the Cl^- trapped in liposomes with wild-type afTMEM16 or the D511A/E514A mutant. **E:** Phospholipid scrambling mediated by afTMEM16 in 0 Ca^{2+} (Black) or with 0.3 mM Ca^{2+} (cyan), Ba^{2+} (red), Mg^{2+} (green), Mn^{2+} (blue), Cd^{2+} (yellow) or Sr^{2+} (pink). Left panel: quantification of scrambling activity measured at t=60s.**F**: Cl- flux mediated by afTMEM16 in 0 Ca^{2+} (Black) or with 0.3 mM Ca^{2+} (cyan), Ba^{2+} (red), Mg^{2+} (green), Mn^{2+} (blue), Cd^{2+} (yellow) or Sr^{2+} (pink). **G** Phospholipid scrambling (left) or Cl^- efflux (right) mediated by the D511A/E514A mutant with 0.5 (red) or 0 (black) mM Ca^{2+}. A_{Fast} and A_{Slow} are shown in (B). * denotes addition of dithionite. ^ denotes the addition of Valinomycin. Arrow denotes addition of detergent. All experiments were repeated at least three times and error bars represent the s.e.m.

3.1.9. Lipid modulation of channel activity in afTMEM16

We noticed that in membranes formed from a 3:1 mixture of POPE and POPG the afTMEM16 channel is poorly active: out of 263 attempts we recorded channel activity only 7 times (2.7% rate of success); these recordings were also brief, with only 3 of them lasting longer than 3 min (**Figure 6**; **Table 1**). In contrast, the flux assays show that the afTMEM16 channel is fully active in liposomes formed from a 3:1 mixture of E. coli polar lipids and egg PC (Coli/PC) (**Figure 7**). We tested whether this different activity was due to the different lipid composition by measuring fluxes mediated by afTMEM16 in liposomes formed from the POPE/POPG mixture. We found that these proteo-liposomes retain most of their Cl^- content regardless of the presence of saturating Ca^{2+} (**Figure 7C**) , 86±4% (n=6) and 69±8% (n=6) respectively in the absence and presence of Ca^{2+}. Thus, in POPE/POPG membranes the channel activity of afTMEM16 is severely inhibited. When we attempted to record afTMEM16 channels in planar lipid bilayers formed from Coli/PC lipids we found that they are unstable, they last < 5 min on average (**Table 1**), and are thus unsuitable for electrophysiological recordings. Despite this, we did see channels with properties similar to those seen in PE/PG bilayers (high conductance and poor selectivity) in 2 out of 18 attempts (11.1% rate of success) (**Table 1**) suggesting that the channel has higher activity in these conditions.

These results suggest that the bulk lipid composition of the membrane is a key regulator of the ion channel activity of afTMEM16. Therefore, we investigated which lipids were required for channel activity. The *E. coli* polar mixture

comprises ~ 67% PE, 23 % PG and 10% cardiolipin[110,111], therefore the main differences between the active E. coli: Egg PC (3:1) mixture and the inactive POPE:POPG (3:1) are the presence of PC and cardiolipin (**Figure 11B**). We performed flux experiments with afTMEM16-containing liposomes made by 100% E. Coli Polar extract or Egg PC and we found that in both conditions the channel was fully active (**Figure 11C**).Thus neither cardiolipin nor Egg PC are strictly required for channel activity. Based on these results we conclude that we can further reduce the complexity of our reconstituted system by using only *E. Coli* Polar extract without Egg PC, as also scrambling is unaffected (**Figure 12B**).

A second key difference between the *E. coli* lipid extract and the 3:1 synthetic mixture of POPE:POPG is that, while the latter contains only one specific acyl chain combination for both (16:0-18:1) the former contains PE with four different acyl chains (16:0-16:1; 16:0-18:1; 18:1-18:1; 14:0-16:1) [110,111] in addition to cardiolipin and PG (**Figure 11B**), resulting in a mixture of phospholipids with variable chain lengths. Thus, we questioned whether the homogeneous acyl chain length of the synthetic mixture influences channel activity. To test this hypothesis we investigated whether perturbations of this homogenous population via addition of other phospholipids could rescue afTMEM16 channel activity. This is the case. When 15-25 % (mole %) PC (extract with the predominant acyl chain being 16:10), PS (18:0-18:0) or cardiolipin (four identical 14:0) is added to a POPE:POPG (3:1) background, afTMEM16-containing liposomes show partial to full recovery of channel activity (**Figure 11 D-F**). There are differences in the % of channel activity rescued: while

15% PC is sufficient to fully recover the activity and 25% PS almost fully restore the activity, 15-25% cardiolipin show less, although significant recovery.

Overall these results show that channel activity of afTMEM16 is influenced by lipids. Although further experiments are required to better understand the lipid requirements, it seems that the lipid modulation of channel activity is fairly nonspecific and it might be related to the acyl chains, rather the head groups, of the phospholipids.

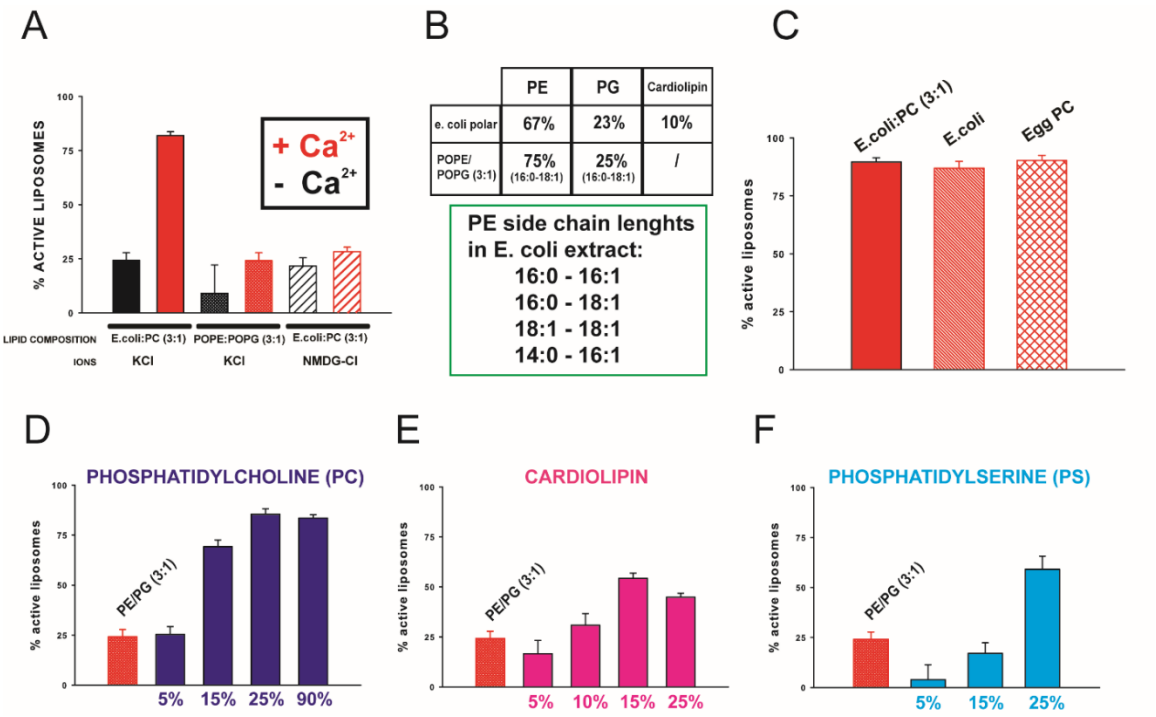

Figure 11: Lipid modulation of ion channel activity.
A: Fraction of trapped Cl^- represented as % of active liposomes normalized to each protein-free condition. Proteoliposomes formed in E. Coli Polar: Egg PC (3:1) or POPE:POPG (3:1) with (red) or without (black) 0.5 mM Ca^{2+} and with KCl or NMDG-Cl. **B**: Lipid composition of E. coli Polar extract (*according to Avanti Polar Lipids*). **C**: % of active liposomes made in E. Coli:Egg PC (3:1), 100% E. Coli polar and 100% Egg PC in the Cl^- flux assay. **D-E-F**: rescue of channel activity with phosphatidylcholine (D), Cardiolipin (E) or phosphatidylserine (F) titrated into a POPE:POPG mixture. All experiments were repeated at least three times. Error bars represent s.e.m.

3.1.10. Ion transport is not required for phospholipid scrambling in afTMEM16

As channel activity was severely reduced in POPE:POPG, we investigated whether this lipid composition also caused inhibition of scrambling. This is not the case. When afTMEM16 is reconstituted in liposomes formed in POPE:POPG (3:1) scrambling still occurs, in a Ca^{2+}-dependent manner, (**Figure 12A**) similarly to what we observed in E. Coli : Egg PC (3:1). The kinetics of fluorescence decay in POPE/POPG liposomes are only ~2-fold slower than those seen in Coli/PC vesicles. Thus, the POPE/POPG membrane scaffold drastically inhibits the channel activity of afTMEM16 but has almost no effect on its ability to scramble lipids, showing that channel and scrambling activities are functionally independent and separable. All the lipid composition tested for channel activity, including 100% E. Coli (**Figure 12B**), did not alter scrambling properties of afTMEM16 , suggesting scrambling is not tightly regulated by lipids, as expected for a non-selective lipid transporter.

We then looked into the relationship between ion and lipid transport. As shown before, $NMDG^+$ acts as impermeant cation (**Figure 7C**). When KCl is substituted with NMDG-Cl scrambling activity of afTMEM16 is not affected (**Figure 12C, E**), reinforcing the hypothesis that ion transport is not required for lipid scrambling to occur. Furthermore, scrambling takes place even in the presence of low salt. When scrambling experiments were performed in the presence of a 30 fold KCl gradient, 300mM inside and 10 mM outside instead of symmetrical 300 mM KCl, scrambling still occurred, at a slower rate (**Figure 12D-**

E). Because dithionite is added 100s after the liposomes are dissolved into the external solution, all the KCl gradient is dissipated during that time thus scrambling is happening in the presence of minimal (if any) ion flux. Together these experiments show that phospholipid scrambling does not require ion permeation to occur.

Overall, these results show that ion and lipid transport are functionally independent and that scrambling can take place in the absence of ion transport. These results suggest that ion and lipid transport are functionally independent, a result that might indicate that the two substrates use separate pathways. Alternatively, ions might permeate through a disturbance in the membrane that underlies lipid scrambling and that specific lipid compositions form tighter seals around afTMEM16, preventing ion transport. Further experiments, for example using mixtures of synthetic phospholipids with different acyl chains, are required to distinguish between these possibilities.

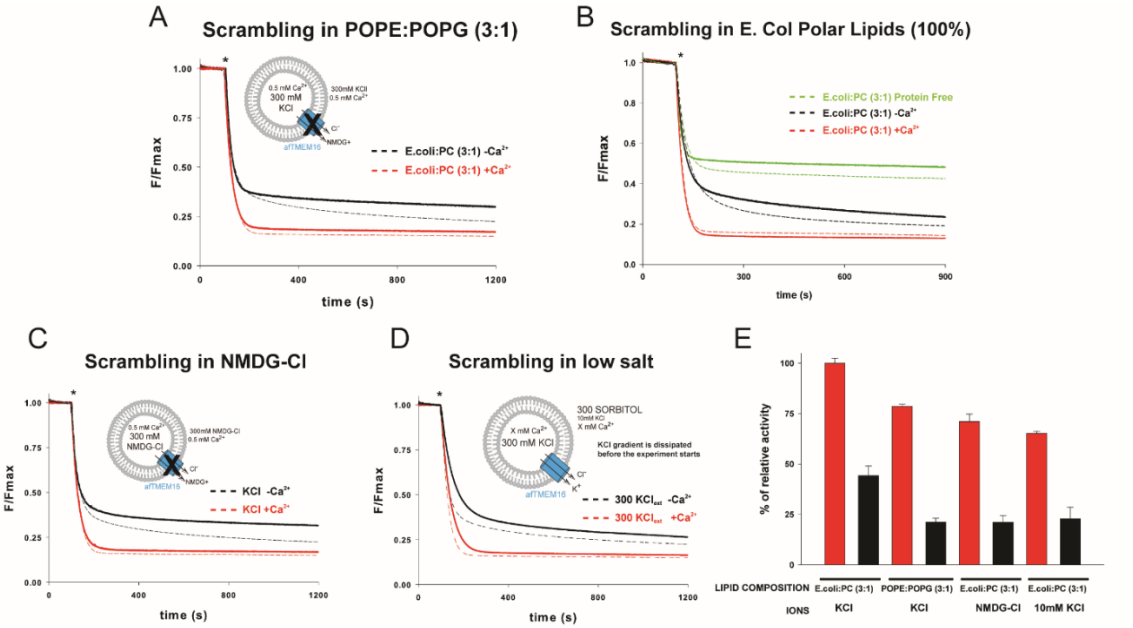

Figure 12: Ion transport is not required for lipid scrambling to occur in afTMEM16.

A: Phospholipid scrambling by afTMEM16-containg liposomes made in POPE:POPG (3:1) in the presence (red) or absence (black) of 0.5mM Ca^{2+}. Dashed lines represent scrambling by proteoliposomes made in E. Coli:Egg PC (3:1). **B**: Phospholipid scrambling by afTMEM16-containg liposomes made in E. Coli Polar lipids in the presence (red) or absence (black) of 0.5mM Ca^{2+}. Dashed lines represent scrambling by proteoliposomes made in E. Coli:Egg PC (3:1). **C**: Phospholipid scrambling by afTMEM16-containg liposomes made in E. Coli:Egg PC (3:1) in symmetrical 300 mM NMDG-Cl, in the presence (red) or absence (black) of 0.5mM Ca^{2+}. Dashed lines represent scrambling in symmetrical 300 mM KCl. **D**: Phospholipid scrambling by afTMEM16-containg liposomes made in E. Coli:Egg PC (3:1) exposed to a solution containing 300mM Sorbitol and 10 mM KCl, in the presence (red) or absence (black) of 0.5mM Ca^{2+}. The KCl is dissipated during the 100s before addition of dithionite. Dashed lines represent scrambling in symmetrical 300 mM KCl. **E**: Quantification of phospholipid scrambling measured at t=60s. Values were normalized to ΔFluorescence of Coli:EGG PC (3:1) liposomes in the presence of symmetrical 300mM KCl. Error bars are the s.e.m.

3.2. Investigating the mechanisms underlying phospholipid scrambling and Ca^{2+} modulation in afTMEM16

3.2.1. The structure of a TMEM16 scramblase identifies a putative lipid pathway and suggests a mechanism for phospholipid scrambling

A major breakthrough in our understanding of phospholipid scrambling by TMEM16 proteins came in January 2015 when Brunner and colleagues solved the crystal structure of a TMEM16 phospholipid scramblase[33] (*see chapter 2.4*). They showed that the fungal homologue nhTMEM16 is a Ca^{2+}-dependent phospholipid scramblase, but not an ion channel, with properties resembling those of afTMEM16: Ca^{2+} dependency, reduced but substantial activity in the absence of Ca^{2+} and broad lipid specificity. nhTMEM16 is 48% identical to afTMEM16, with >70% homology within the transmembrane regions. The structure identified a hydrophilic cavity (groove), ~8-11 Å wide, exposed to the hydrophobic core of the membrane as the putative lipid pathway. It was proposed that lipid scrambling occurs via phospholipid headgroup-protein interactions within the cavity in a bi-directional, semicircular fashion (**Figure 4**). The model predicts that lipids with head groups larger than the width of the cavity should not be translocated. To test the lipid translocation model proposed by the Dutzler group we investigated whether there is a size cut-off for the phospholipid head group. We generated NBD-labelled PE phospholipids with polyethylene glycol (PEG) molecules of increasing size attached to the headgroup (*see methods*) and monitored scrambling by afTMEM16.

3.2.2 Characterization of NBD-PEG phospholipids

We generated the NBD-PEG phospholipids by attaching the NBD group to a DSPE-PEG (*see methods*). The resulting product is a phospholipid with a PE headgroup, a PEG molecule and the NBD fluorophore (**Figure 13A**). We started with PEG 1000, 2000 and 3400. We first confirmed the purity of the products by mass spectrometry and measured the average diameter of the PEGs in aqueous solution by dynamic light scattering (DLS). We found that PEG1000 has an average diameter of ~ 3 nm; PEG2000 of ~ 4 nm and PEG3400 of ~ 5 nm (**Figure 13B**). Thus all three PEGs have size larger than the lipid cavity (0.8-1.1nm). We then tested whether these products were stable when reconstituted in liposomes and we found that protein-free liposomes containing PEG1000 or PEG 2000 (0.5 mole%) showed the expected 50% loss of fluorescence (**Figure 13C**), ruling out the possibility of the liposomes being unstable or the NBD-PEGs not being incorporated. Interestingly, we noticed a difference in the kinetics of dithionite reduction. When compared to NBD-PE we found that while NBD-PEG1000-containing liposomes showed similar kinetics (15.3 ± 0.6s and 14.8 ± 1.4s), the time constant liposomes containing NBD-PEG2000 is ~1s, similar to the one for free NBD in solution (**Table 2**, **Figure 13D**). As The NBD group is attached to the PEG, which has an average diameter of ~4nm in the case of PEG2000 (**Figure 13B**), this suggest that the NBD group is now fully exposed to the outer solution and dithionite can reduce it as fast as free NBD. Thus we think that the slower kinetics observed in our NBD-PE experiments are cause by the NBD group not being fully exposed to the aqueous solution but instead being

partially buried within the membrane. This will become relevant in the next chapters for the discussion regarding the scrambling rate with NBD-PEG phospholipids.

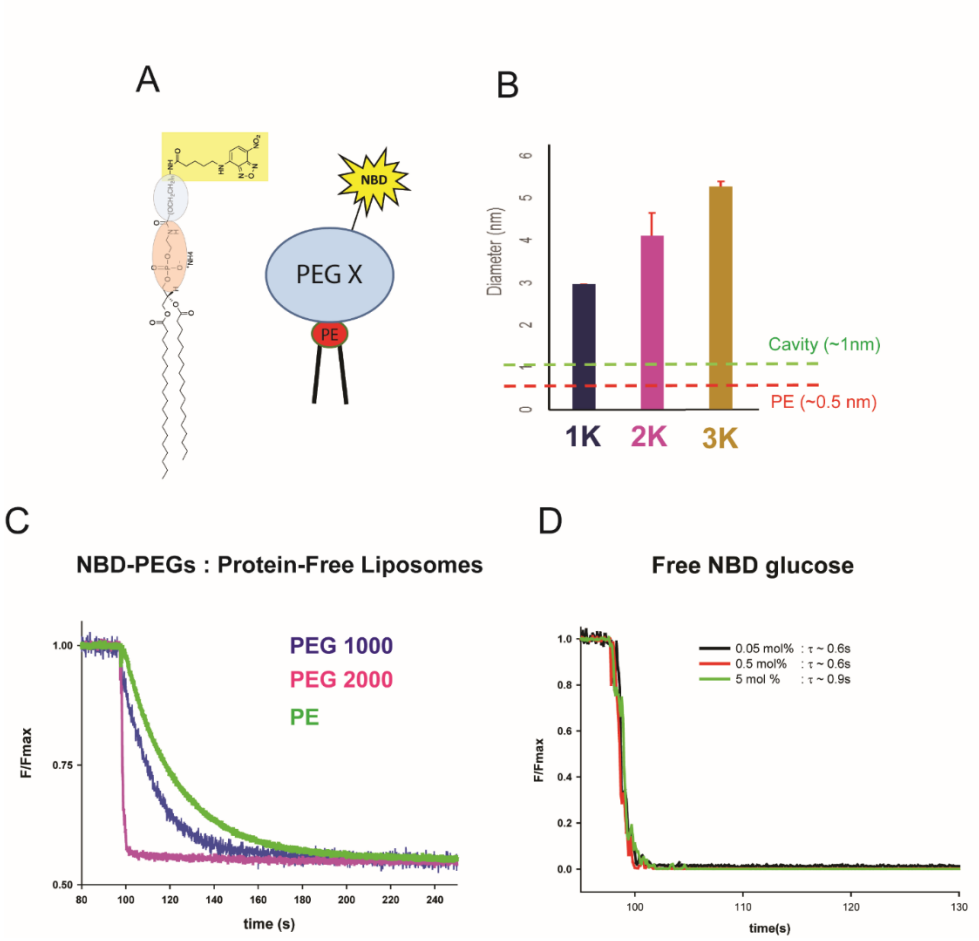

Figure 13: Characterization of NBD-PEG phospholipids.
A: Structure of a NBD-conjugated DSPE-PEG. **B**: Dynamic light scattering measurements of NBD-PEG1000; 2000 and 3400. Average values of the nhTMEM16 subunit cavity width (green) and the diameter of the headgroup of a phosphatidylethanolamine (PE, red) are shown as dashed lines. **C**: Fluorescence loss by protein-free liposomes containing 0.5 mole% of NBD-PE (green), NBD-PEG1000 (blues) and NBD-PEG2000 (pink) upon dithionite addition at t=100s. For clarity only the first 250s of the time courses are shown. Average time constants can be found in *Table 2*. **D:** Fluorescence loss of free NBD-glucose in solution (300mM KCl, 50 mM HEPES pH7.4, 0.5 mM $Ca(NO_3)_2$ at three different concentration (black: 0.05 mole %, red: 0.5 mole %, green : 5 mole %). Time courses were fit to a single exponential function and the times constants were 0.6s (0.05%), 0.65s (0.5%) and 0.91s (5%).

3.2.3. Interactions within the lipid pathway are not strictly required for lipid scrambling to occur.

When incorporated in trace amounts (0.5 mole %) into afTMEM16-containing liposomes, in the presence of Ca^{2+}, all three PEG1000, 2000 and 3400 are scrambled (**Figure 14A**). The steady-state values are comparable with that of NBD-PE and the kinetics of dithionite reduction are similar in the case of PEG1000 and faster for PEG2000 and 3400 (*see chapter 3.2.5 and Table 2* for a discussion of the kinetics). These results show that increasing the headgroup size has almost no effect on the ability of afTMEM16 to scramble lipids. As the measured diameter for the PEGs indicate that the headgroup are larger than the width of the cavity by 2-4 nm, we can conclude that the cut-off for phospholipid headgroup is larger than expected from the structure. Furthermore, our results suggest that tight interactions between head groups and the protein within the cavity are not strictly required for scrambling to occur.

3.2.4. Opening transitions can occur in the absence of Ca^{2+}.

One of the most interesting properties of afTMEM16 is the substantial activity observed in the absence of Ca^{2+} (**Figure 8**). While Ca^{2+} does increase the scrambling rate by >20 fold, scrambling still occurs, at a significant slower rate, in the absence of Ca^{2+}. The same result was shown for nhTMEM16 with almost identical kinetics[33]. The simplest model that accounts for this observation is that the scramblase has an open and a closed state, and that the opening rate is non-zero even in the absence of ligand (**Figure 14B**). An alternative

explanation would be that in the apo state the pathway does not completely close so that there is a non-zero basal conductance for lipids. In this model, Ca^{2+} binding would induce a widening of the pathway leading to an increase in the lipid translocation rate (**Figure 14B**). We reasoned that these two models could be differentiated based on the size cut-off of the two states. If the scramblase has an open and a closed states then we would expect that the scrambling in 0 and saturating Ca^{2+} has the same selectivity. Conversely, the second model predicts that scrambling in 0 and in high Ca^{2+} has different size cut-offs. Our results are consistent with the hypothesis that there is one conductive state and that the apo state can visit the open conformation even in the absence of Ca^{2+}, explaining the scrambling activity in the absence of Ca^{2+}. When afTMEM16-containing liposomes with NBD-PEG2000 were assayed for scrambling activity in the absence of Ca^{2+} they showed rates comparable to NBD-PE (**Figure 14D-E**). After the initial drop around 50% (reduction of the outer leaflet) with a time constant of ~1s there is a slow ‘’leak’’ which can be fit with a polynomial function from which we estimate the time constant to be ~1000s with a relative weight of 0.09 ± 0.02, which is only a two-fold increase from the ~400s observed with NBD-PE. (**Table 2**). It is important to notice that in the presence of Ca^{2+} we are starting to separate the NBD reduction from the scrambling process, which is one important limitation in our estimate of the scrambling rates with NBD-PE. The decay is now well fit with a double exponential function with a fast component with a time constant of ~ 1s and a slow component with a time constant of ~15s. The fast component represents the NBD reduction by dithionite and the slow

component represents the scrambling process. This will be discussed in more details in the next chapter. When the scrambling rates are calculated, with the slow time constant of ~15s in the presence of Ca^{2+} which represents scrambling, we see that Ca^{2+} increases the scrambling rate by ~80 fold. This, under the approximations used to estimate the scrambling rate, is not significantly different from the >20 fold increase observed for NBD-PE, especially considering the in the presence of Ca^{2+} we are limited by the chemistry due to NBD reduction by dithionite, thus the rate in the presence of Ca2+ is likely to be faster. Thus the apo and bound states have similar size selectivity, consistent with a model according to which there is one conductive state and the protein can visit the open conformation even in its unligaded state.

Consistent with this hypothesis, PEG1000 also gave us results comparable to NBD-PE (**Figure 14C**). In the presence of Ca^{2+} the time constant of the fluorescence decay is ~15s and in the absence of Ca^{2+} the fluorescence loss is well fit with a double exponential with time constant of ~600s and relative weight of 0.15 (**Table 2**), resulting in Ca^{2+} increasing the scrambling rate by ~40 fold, similar to what observed for NBD-PE liposomes.

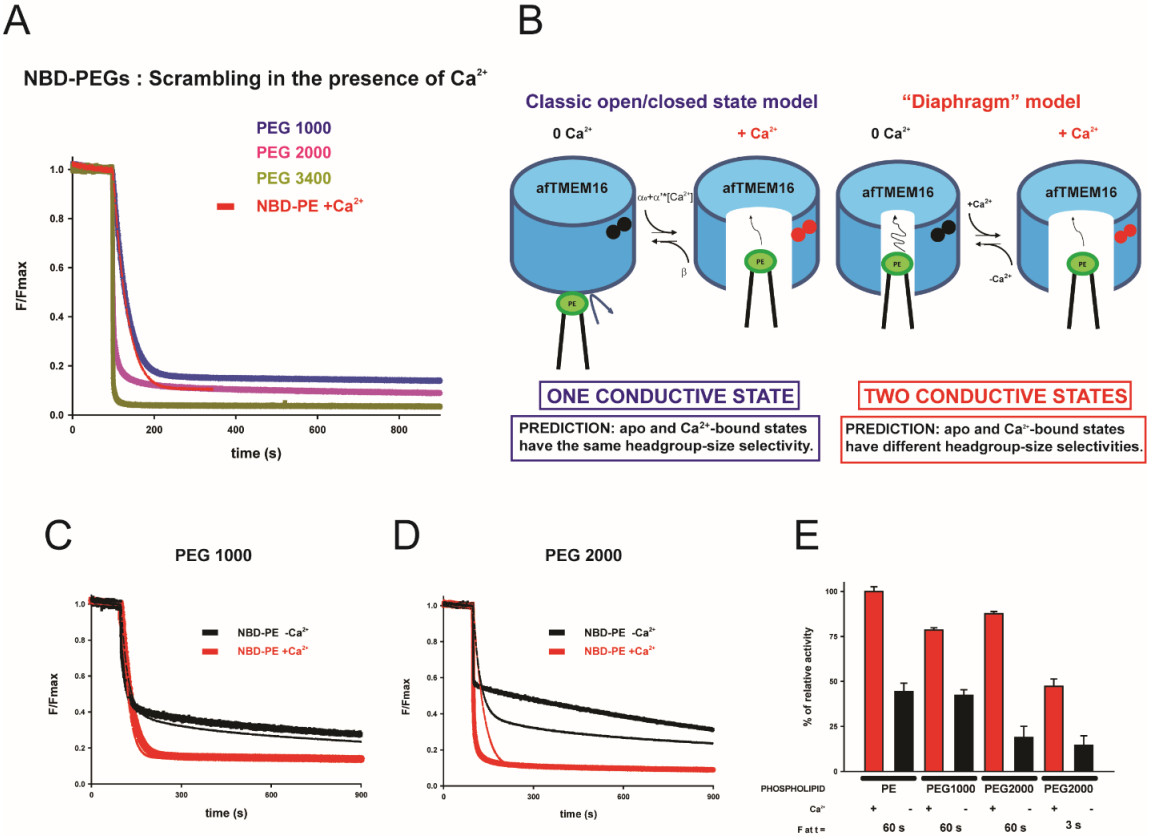

Figure 14: Scrambling with NBD-PEGs
A: Phospholipid scrambling by afTMEM16-containing liposomes in the presence of 0.5 mM Ca^{2+} with NBD-PEG1000 (blue), 2000 (pink) and 3400 (dark yellow). A representative trace of scrambling of afTMEM16-containing liposomes with NBD-PE is shown as red dashed line. **B**: Cartoon representing two possible models that may explain the substantial scrambling activity in the absence of Ca^{2+}. Spheres represent the presence (red) or absence (black) of Ca^{2+} ions bound to the protein. **C-D**: Phospholipid scrambling by afTMEM16 with NBD-PEG1000 (D) or NBD-PEG2000 (E) in the presence (red) or absence (black) of Ca^{2+}. Dashed lines represent scrambling with NBD-PE. **E**: Scrambling activity measured at t=60s or t=3s (for NBD-PEG2000 only). All experiments were performed with liposomes made in E. Coli Polar lipids. At least 3 independent experiments for each conditions were performed. Error bars are the s.e.m.

3.2.5. Analysis of the scrambling rates with NBD-PEG2000

An important observation from our NBD-PEG2000 experiments is that the time constant in the presence of Ca^{2+} is different from that observed in the NBD-PE experiments (**Figure 13C, Figure 14A**). While the time course of fluorescence loss in NBD-PEG2000 protein-free liposomes is well fit with a single exponential with time constant similar to that of free NBD in solution (~1s), fluorescence loss of NBD-PEG2000 in afTMEM16 proteo-liposomes in the presence of Ca^{2+} is well fit by a double, rather than a single, exponential function (**Figure 15A, Table 2**). This is different from our NBD-PE experiments where fluorescence loss in the presence of Ca^{2+} is well fit with a single exponential function with time constant similar to that of protein-free liposomes (**Figure 8, Figure 15B, Table 2**). In liposomes with NBD-PEG2000 the fast component is predominant, ~68%, with time constant of ~0.7 s, comparable to the one of the protein free-liposomes and the free NBD. The weight of the slow component is less but significant, ~18%, with a time constant of 18s (**Figure 15, Table 2**). The appearance of a second, slower component with time constant different from that of protein-free liposomes (which represents the time constant due to the chemical reaction of dithionite reduction of NBD-groups) shows that in the presence of Ca^{2+} scrambling is starting to become separate from the chemical reduction of NBD groups, which is the rate-limiting step in our NBD-PE experiments. This is readily visualized when we compare scrambling activity of proteo-liposomes with NBD-PEG2000 in the presence of Ca^{2+} at $t=3*\tau$ of the protein free NBD-PE (60s) and NBD-PEG2000 (3s) liposomes. After 60s all the

outer leaflet is completely reduced and the % of activity is ~90% of that of NBD-PE (**Figure 14C**), but this value is based on the τ of NBD-PE liposomes and it is 60 times the time constant of the outer leaflet reduction with NBD-PEG2000, which is ~1s. When scrambling is measure at t=3*τ of the NBD-PEG2000 protein free- liposomes, the activity of afTMEM16-containing liposomes in the presence of Ca^{2+} drops to ~50% (**Figure 15C**). This shows that, different from what we observed with NBD-PE, scrambling is still occurring at t=3*τ of the outer leaflet reduction, thus the chemical reduction of NBD groups and phospholipid scrambling are separated.

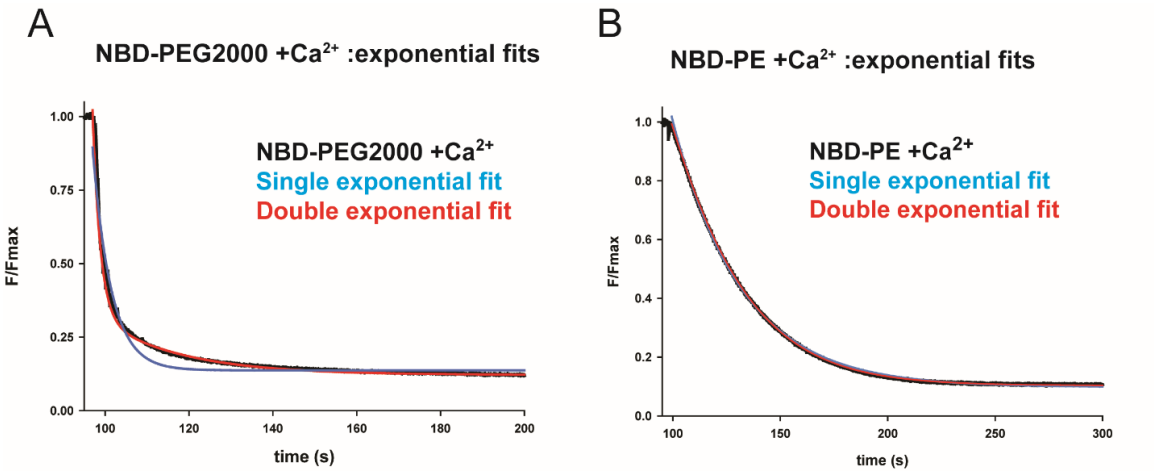

Figure 15: Comparison of the fluorescence loss between NBD-PE and NBD-PEG2000.
A-B: Comparison between single (light blue) and double (red) exponential fits of the time course of fluorescence loss in afTMEM16-containing liposomes with NBD-PEG2000 (B) and NBD-PE (C), in the presence of 0.5mM Ca^{2+}. For clarity only the first 200s (B) and 300s (C) of the time courses are show. The time course was fit to $^{F}/_{F_{Max}} = A_0 + A_{Fast}e^{-t/\tau_{Fast}} + A_{Slow}e^{-t/\tau_{Slow}}$ where A_0 is an offset needed to account for the fraction of refractory liposomes, $A_{Fast(Slow)}$ is the relative weight of the fast (slow) component of the decay and $\tau_{Fast(Slow)}$ is its relative time constant. For single exponential fit the $A_{Slow}e^{-t/\tau_{Slow}}$ term is 0.

Table 2: **analysis of scrambling kinetics**

Liposomes were formed in E. Coli Polar lipids with 0.5 mole % of NBD-PE, PEG1000 or PEG2000. The times courses were fit to $F/F_{Max} = A_0 + A_{Fast}e^{-t/\tau_{Fast}} + A_{Slow}e^{-t/\tau_{Slow}}$ where A_0 is an offset needed to account for the fraction of refractory liposomes, $A_{Fast(Slow)}$ is the relative weight of the fast (slow) component of the decay and $\tau_{Fast(Slow)}$ is its relative time constant. For single the exponential fit the $A_{Slow}e^{-t/\tau_{Slow}}$ term is 0. Average values are representative of at least three independent experiments.

	τ protein-free (s)	**Ca^{2+}**	**τ_{fast} (s)**	**A_{fast}**	**τ_{slow} (s)**	**A_{slow}**
PE	15.3 ± 0.6	+	18.9 ± 0.9			
		-	18.3 ± 1.3	0.57 ± 0.01	400 ± 18.5	0.19 ± 0.01
PEG 1000	14.8 ± 1.4	+	15.6 ± 0.7			
		-	14.5 ± 0.6	0.5 ± 0.04	600 ± 25	0.15 ± 0.018
PEG 2000	1.1 ± 0.1	+	1.6 ± 0.2	0.68 ± 0.03	15.1 ± 1.2	0.18 ± 0.02
		-	1.2 ± 0.09	0.6 ± 0.03	1200 ± 98	0.09 ± 0.02

4. Discussion

We identified and purified a novel homologue of the TMEM16 family, afTMEM16, and showed that is a dual-function protein: it is a Ca^{2+}-gated ion channel and a Ca^{2+}-dependent phospholipid scramblase. This was the first time that a member of the TMEM16 family was directly proved to be the molecular counterpart of the long sought phospholipid scramblases. After our initial discovery of afTMEM16 the crystal structure of nhTMEM16 was solved allowing for the formulation of initial mechanistic hypotheses on how lipid scrambling occurs. These structural and functional results also posed numerous questions as to how channel and scrambling activity can co-exist within the same family and what structural and biophysical properties underlie the functional differences observed among TMEM16 members.

4.1. afTMEM16 as a Ca^{2+}-gated ion channel

afTMEM16 is a Ca^{2+}-gated, non-selective ion channel displaying voltage dependence (**Figure 6, 7**). The poor ion selectivity, P_{K^+}/P_{Cl^-} ~1.5, is consistent with what has been observed for other TMEM16 channels. The most selective TMEM16 channels, A and B, do not have in fact strong ion selectivity: P_{Cl^-}/P_{X^+}~7[27,75]. Furthermore, it was shown for both that the anion selectivity changes during channel activation[27]. It is harder to compare the activity of afTMEM16 to channel activity described for TMEM16F, mainly because it is not clear what type of channel TMEM16F is. If we consider the reports suggesting that it is an anion channel, these also show that it has significant cation permeability, with P_{Na^+}/P_{Cl^-}

ranging from 0.3 to 6.7 depending on the study [87,89]. TMEM16F as a cation channel, which Yang and colleagues described as a non-selective cation channel, also appears to be poorly selective with P_{K^+}/P_{Cl^-}~ 7, and a point mutation further decreased the selectivity to ~2 [77]. Finally, recent reports suggested that TMEM16F, similar to afTMEM16, is a non-selective channel with P_{Na^+}/P_{Cl^-} ~1.4 or ~0.5[30,31]. Overall, these reports suggest TMEM16F has a non-selective pore and that this is a property shared by all TMEM16 channels. The disagreement regarding the ion selectivity of TMEM16F might be caused, similarly to TMEM16A and B, by the selectivity changing during channel activation.

The pore of afTMEM16 is large. We found TEA^+ can go through the channel while $NMDG^+$ does not, suggesting the narrowest region of the pore is between 4 and 6.5 Å. This is consistent with the data suggesting TMEM16F has a large ion pore as well, as it was shown that the channel is permeable to $NMDG^+$ [77] thus indicating the pore may be larger than 6.5 Å.

4.2. afTMEM16 as a Ca^{2+}-dependent phospholipid scramblase

afTMEM16 is a Ca^{2+}-dependent phospholipid scramblase, with properties resembling those of native scramblases: Ca^{2+}-dependency, rapid transport and poor lipid selectivity. Removal of Ca^{2+} slows afTMEM16-mediated scrambling by >20-fold from >10^4 to ~400 lipid s^{-1} (**Figure 8**). Our data show that K_m^{app} for Ca^{2+} is ~0.4 mM. It is important to note that afTMEM16 retains substantial activity in the absence of Ca^{2+}. The same was observed for the other fungal homologue

nhTMEM16[33] and it will be discussed later (*see chapter 4.7*). It is important to notice that these are estimate as we are not able to calculate precisely the scrambling rate in either states: in the presence of Ca^{2+} we are limited by the chemical reaction of dithionite reduction, in 0 Ca^{2+} the decay of fluorescence is too slow and it would require longer experiments. We also found that afTMEM16 mediates the Ca^{2+}-dependent transport of a variety of lipids with different headgroup properties, albeit at different rates: NBD-PS, NBD-PE as well as PE bearing the NBD fluorophore on the headgroup (N-NBD-DPPE), NBD-PC, NBD-glucosylceramide and the cationic lipid DOTAP (**Figure 8**). When we quantify phospholipid scrambling at t=60s (3*τ) compared to NBD-PE we see that all lipids are translocated in the presence of Ca^{2+} and scrambling is Ca^{2+} dependent (**Figure 8**), as expected from what was reported for native phospholipid scramblases[10].

4.3. A common Ca^{2+}-binding region regulates both ion and lipid transport in afTMEM16

afTMEM16 is a Ca^{2+}-dependent dual function channel/scramblase. We found that the same Ca^{2+}-binding region regulates both processes. Our measurements show that the K_m^{app} for Ca^{2+} is ~0.4 mM (**Figure 9**). Both functions share the same apparent divalent selectivity: Ca^{2+} > Mn^{2+} ~ Sr^{2+} > Ba^{2+}> Cd^{2+} ~ Mg^{2+}. Charge neutralization of the di-acidic motif (D511A/E514A) located in one of the intracellular loops nearly abolishes the Ca^{2+} dependence of channel and scrambling activities. The same region, which is among the highest

conserved regions within the TMEM16 family, was previously reported to alter Ca^{2+}-sensitivity in TMEM16A and F[75,77], thus our data further supported the hypothesis of TMEM16 proteins sharing the same Ca^{2+}-binding site and proved that Ca^{2+} can bind directly to TMEM16 proteins. These results were then confirmed by the nhTMEM16 structure[33] which shows two Ca^{2+} ions bound (per monomer) to a Ca^{2+}-binding region comprising residues in TM 6-7-8: three glutamates (E506, E535 and E452), two aspartates (D503 and D539) and one asparagine (N448) (**Figure 4**). As expected, these are the residues previously identified in TMEM16A and F[75,77,112]. Interestingly, the Ca^{2+}-binding site resides within the membrane, right behind the lipid pathway, and this explains the voltage dependence of Ca^{2+} activation seen for TMEM16 proteins[25,27,77,78,96] as ions have to travel almost half way through the membrane.

The double mutant E511A/D514A shows little, Ca^{2+}-indipendent, residual scrambling activity. Interestingly, it is much lower than the activity observed in wild type afTMEM16 in the absence of Ca^{2+}. As the location of the binding site is adjacent to the lipid pathway (in fact helix 6 participates to forming both the lipid pathway and the Ca^{2+}-binding site) and our mutations are drastic (E/D to A) this might cause the structure to locally collapse, directly affecting the lipid pathway. As a result scrambling would be altered and this is reflected by lower activity in 0 Ca^{2+}.

4.4. Are the ion and lipid pathways separate in afTMEM16?

The observation that a common Ca^{2+}-binding site regulates the two transport activities of afTMEM16 raises the question of whether the ion and lipid pathways are separate or share a common pathway. Although we do not have a definitive answer, our data showed that the two functions are independent and can be separated. We found that by changing the lipid composition of the liposomes from E. coli polar lipids to POPE:POPG (3:1) we were able to almost abolish channel activity leaving scrambling unaltered (**Figure 11, 12**). This suggests ion transport is not required for lipid scrambling to occur, consistent with our data showing that scrambling still occurs even in the presence of the impermeant $NMDG^{+}$. These results suggest, but do not prove, that ion and lipid pathways are separate in afTMEM16. If that is the case, one possible explanation might be that the more rigid structure of the liposomes when synthetic POPE and POPG are used, compared to the E. coli mixture (which contains PE with at least four different acyl chains), might prevent a conformational change required for channel gating. This would be consistent with our findings that 15%-25% Egg PC, cardiolipin or PS in a POPE/POPG (3:1) background is sufficient to rescue channel activity (**Figure 11**).

4.5. Ion and lipid pathways in TMEM16 proteins

A groundbreaking result for the field came in January 2015 when the first crystal structure of a TMEM16 scramblase was solved[33] (*see chapter 2.4*). While it confirmed some of the features us and others already showed, such as the

dimeric architecture [94,95] and the location of the Ca^{2+}-binding region[75,77,112], it also identified the putative lipid pathway: a hydrophilic cavity, 8-11 Å wide, exposed to the membrane. The structure poses the fundamental question of whether ions and lipids share the same pathway or have two separate pathways in TMEM16 proteins. As mentioned before, it is important to notice that we have convincing evidence suggesting that nhTMEM16 is a dual function channel/scramblase as well. One hypothesis is that ions leak through the lipid pathway as a consequence of lipid scrambling, thus sharing the same pathway with the phospholipids. This is mostly based on the mutagenesis analysis on TMEM16A. Many amino acids showed to be involved in TMEM16A ion selectivity seem to reside along the nhTMEM16 cavity. Four basic residues, equivalent to R515, K603, R621 and R788, alter anion selectivity in TMEM16A and, when mapped onto the nhTMEM16 structure, all four residues cluster in the top region of the cavity[113]. The single K588Q mutation doubles the Na^+ permeability in TMEM16A and lies in the cavity[25]. Furthermore, a number of amino acids between G628 and Q637 in TMEM16A, located within the cavity, altered anion selectivity in cysteine-reactive MTS experiments[75] . After the recent discovery that TMEM16F seems to be a dual function channel/scramblase, it was proposed that the cavity serves as the ion and lipid pathway in TMEM16F[31,97] in a model where the ions leak as consequence of lipid scrambling. This is further corroborated by the findings that TMEM16A can be turned into a phospholipid scrambling by swapping only 15 amino acids from the equivalent region of TMEM16F[31] . This strongly suggests that the structural differences between

TMEM16 channels and scramblases are local and subtle, thus it is unlikely that the structure of a TMEM16 ion channel will differ significantly from the nhTMEM16 structure. The cavity would provide half the hydrophilic environment while the headgroups of the phospholipids would provide the other half, allowing ions to move through a ‘’broken’’ pore. While corroborated by mutagenesis analysis in TMEM16A, this fascinating hypothesis has some potential problems. First, the residues where mapped by homology modelling but we do not know if these residues are indeed within the cavity in TMEM16A, as homology between TMEM16A and nhTMEM16 is low (<30%). Indeed, there are some selectivity-altering mutations in TMEM16A which do not seem to be located along the lipid pathway[25]. Second, if ions leak through the lipid cavity as a consequence of phospholipid scrambling, how is it possible to achieve ion movement in TMEM16A, a channel with no scrambling activity? Third, while afTMEM16 and possibly nhTMEM16 and TMEM16F are poorly selective channels, TMEM16A and B show preference (although not strong) for anions over cations. While it seems plausible for a dual function protein to behave as a non-selective channel, it is a non-selective lipid scramblase so that lipids with different headgroups could act as counterbalance charges for opposite ions, it is hard to envision a situation where TMEM16A and B somehow have positively charged phospholipids surrounding the pathway most of the time. One possible explanation would be that in non-selective channels/scramblases ions and lipids share a common pathway where ions leak as a consequence of phospholipid scrambling while TMEM16 channels evolved in such a way that the cavity becomes partially

occluded, excluding lipids and providing ion selectivity. The TMEM16A-F chimera experiments suggests that the bottom region of the cavity might be the location where the lipid pathway becomes partially occluded[31]. This would be consistent with our findings of the two functions being functionally independent in afTMEM16, where ion transport is not required for scrambling to occur and does not influence scrambling activity. Clearly a structure of a TMEM16 ion channel would be greatly beneficial to better understand the structural differences underlying channel and scrambling activities in TMEM16s.

4.6. Lipid translocation does not require tight interactions within the lipid pathway

A model for lipid translocation was proposed based on the nhTMEM16 structure: interactions within the cavity between the phospholipid head groups and cavity-forming residues would allow lipids to be translocated in a bi-directional, semicircular fashion (**Figure 4**). We tested this model by studying how scrambling is affected by lipid headgroup size in the presence of Ca^{2+} and we found that the size cut off is larger than expected from the 8-11 Å wide cavity observed in the structure. Our results with NBD-labelled PEGs show that even a PEG3400, which has and average diameter of ~ 5 nm, does not affect scrambling in afTMEM16, which occurs similarly to what we observed for standard physiological phospholipids (**Figure 14**). These results suggest that lipid translocation does not require tight interactions within the cavity to occur. One possible explanation is that the cavity is not providing a ‘’lipid selectivity

filter'' per se but rather it is perturbing the membrane, possibly even fusing the two leaflets, allowing bi-directional lipid translocation to happen without the need for interactions inside the cavity. Thus phospholipid scrambling might be due to the scramblase causing the membrane to become locally unstable rather than a consequence of phospholipid-protein interactions.

4.7. Mechanisms underlying Ca^{2+} modulation of phospholipid scrambling

One of the most interesting properties of phospholipid scrambling in both afTMEM16 and nhTMEM16 is the substantial scrambling activity displayed in the absence of Ca^{2+} (**Figure 8**)**.** While Ca^{2+} does increase the rate of scrambling by >20 fold in afTMEM16, when Ca^{2+} is chelated by EGTA scrambling still occurs, ~400 lipid/s for NBD-PE, suggesting the pathway retains a non-zero conductivity for lipids in the absence of the ligand. There are two main models that could account for this observation (**Figure 14**). The simplest model is that the scramblase has an open and a closed state, similar to what is normally observed for ion channels, and that the opening transition occurs at a finite rate even in the absence of ligand. Alternatively, it is possible that in the apo state the pathway is not fully closed, retaining a non-zero conductance for lipids and Ca^{2+} binding would induce a widening of the pathway leading to an increase in the lipid translocation rate. We reasoned that these two models could be differentiated based on the size cut-off of the two states. If the scramblase has an open and a closed state then we would expect that the scrambling in 0 and saturating Ca^{2+} has the same selectivity. Conversely, the second model predicts that scrambling

in 0 and in high Ca^{2+} has different size cut-offs. Our PEG-based experiments show that increasing the headgroup size does not significantly affect the scrambling rate in 0 and high Ca^{2+}. Experiments performed with NBD-PE showed a >20 fold increase in the scrambling rate by Ca^{2+} and even with the bulkier NBD-PEG2000 Ca^{2+} increases the rate by ~80 fold, thus there is only a 4-fold difference between a standard phospholipid and a PEG2000. It is important to notice that this difference might be even smaller as with NBD-PE we are limited by the chemistry of NBD reduction by dithionite, therefore the rate in the presence of Ca^{2+} could be higher.

These results are consistent with a model according to which there is one conductive state but the protein, in the absence of Ca^{2+}, can visit the open conformation thus providing a possible explanation to the substantial activity observed in the absence of Ca^{2+} in afTMEM16. It is still not clear why scramblases need to have such high activity in the absence of ligand. One possible explanation is that when the Ca^{2+} levels inside the cells are not sufficient to fully activate scramblases might be confined to specific regions of the membrane (such as lipid rafts) where the scramblase is made completely inactive by the lipid composition in which it is embedded. Upon raises in the intracellular Ca^{2+} concentration the protein would relocate within the membrane to a different region where it is not inactivated by certain lipids, becoming fully active. Therefore the cell would not need to be concerned by high activity in 0 Ca^{2+}. We still do not know the actual role of scramblases in lower unicellular organisms such as *Aspergillus fumigatus* and *Nectria haematococca* and it might

be different from what we know for scramblases in higher organisms. A simpler explanation is that scramblases are also regulated by other cellular mechanisms that might involve for example phosphorylation cascades, which we might be missing in reconstituted systems. Further experiments aimed to understand the physiological role of phospholipid scrambling in unicellular organisms are required to better understand the non-zero lipid conductance in the absence of Ca^{2+}.

5. Conclusions

Our finding that the fungal homologue afTMEM16 is a dual function, Ca^{2+}-dependent channel/scramblases was the first proof that members of the TMEM16 family are phospholipid scramblases as well as ion channels. This helped solving the controversy surrounding the role of TMEM16 proteins in phospholipid scrambling and suggests that human TMEM16 proteins might be dual function proteins, as more recent findings on TMEM16F confirmed. Whether ions and lipids share a common pathway or not is still unclear, but our results show that the two functions are functionally separable. Specifically, ion transport is not required for scrambling to occur. As the two functions are regulated by the same, highly conserved Ca^{2+}-binding site this might suggest that TMEM16 Ca^{2+}-activated Cl^- channels, such as TMEM16A, might have evolved from ancestral dual function proteins by blocking lipid transport. Indeed, it has been shown that it is possible to convert TMEM16A, a CaCC, in a scramblases by swapping 15 residues from TMEM16F, suggesting that the structural differences between channels and dual function channel/scramblases are minimal. Thus, the ability of TMEM16 proteins to move either substrates or only ions is likely to reside in local differences that partially occlude the pathway, preventing lipids but not ions permeation.

Our results also suggest that mechanism of phospholipid scrambling might be different from what was proposed based on the structure of the nhTMEM16 scramblase: there is little to no requirement for tight interactions between the phospholipid head-groups and the lipid pathway as shown by the ability of

afTMEM16 to scramble phospholipids with head groups ~ 5 times larger than the width of the cavity in the presence of Ca^{2+}. This suggests that the protein might be perturbing the membrane, possibly fusing the two leaflets, rather than creating a specific lipid pathway. Finally, the observation that the Ca^{2+}-bound and apo states have similar headgroup size selectivities led us to propose a model where in the apo state opening transitions can occur at a finite rate allowing phospholipid scrambling to occur even in the absence of Ca^{2+}. This might explain the substantial activity observed in the absence of Ca^{2+}. While the physiological role of non-zero scrambling activity in the absence of Ca^{2+} remains unclear, it is possible that other proteins or lipids in living cells might further regulate this process, for example by completely silencing scrambling in 0 Ca^{2+}. As we do not know the role of afTMEM16 in the native organism, the fungus *Aspergillus fumigatus*, it is also possible that human scramblases have evolved to completely abolished phospholipid scrambling in 0 Ca^{2+} and that this is only a property of TMEM16 scramblases found in lower organisms. While it is still not clear whether ions and lipids share a common pathway, if this is the case and the lipids are actively involved in ion transport as proposed, this would establish a new way to form ion channels where the membrane is part of the ion pathway. Conversely, if ions and lipids permeate through separate pathways it will be interesting to understand where the ion pathway is located and how channels have evolved from dual function channel/scramblases.

6. Future Directions

In the next future we will focus on gaining further insights into the mechanisms underlying phospholipid scrambling, building on our findings with the PEG experiments. From our experiments it seems that phospholipid scrambling does not require tight interactions within the lipid cavity to occur in afTMEM16, as shown by NBD-PEGs with diameter up to ~5 nm being scrambled as standard, smaller phospholipids in the presence of Ca^{2+}. We will expand our phospholipid headgroup size selectivity analysis. We will test whether bigger PEGs such as PEG5000 and PEG10000 can still be translocated in the presence of Ca^{2+}. If this is the case, then it will further support the hypothesis that the cavity does not act as a lipid ‘’pore’’ but as a facilitator for moving lipid, perhaps by locally distorting the membrane. We will also investigate scrambling in the absence of Ca^{2+}. One possible limitation with this approach is that PEG molecules are flexible and the protein might catalyze the unwinding of the PEG, therefore the bulk portion of the PEG is not going through but rather a small linear part of it. To prevent this possibility we are working to generate NBD-labelled phospholipids conjugated with fullerenes, molecules made of carbon in the form tubes, ellipsoids and spheres. We are focusing specifically on spherical fullerenes (Buckminsterfullerenes[114]). This will allow us to have a rigid modified headgroup and therefore we will be able to better control the size of the probe.

Our NBD-PEG experiments showed that, in the presence of Ca^{2+}, we started to separate the chemical reaction for NBD reduction by dithionite from the scrambling process, as seen with the appearance of a second kinetic

component. We will further investigate this by measuring the temperature dependence of phospholipid scrambling. If the chemical reaction and the scrambling have two distinct Q_{10}, then by lowering the temperature we should be able to further separate the two process, therefore gaining kinetic information on the phospholipid scrambling mechanism.

7. Methods

Cloning and purification of afTMEM16

We renamed the *Aspergillus fumigatus* AFUA_4G02970 (*Aqy1*, PubMed gene ID: 3504033) to afTMEM16 for consistency with other TMEM16 proteins. The afTMEM16 and Ist2p genes were codon-optimized for over-expression in yeast (GenScript, USA), cloned into the *Saccharomyces cerevisiae* Uracil-selectable yEGFP-fusion vector pDDGFP2 [40] and expressed as C-terminally yEGFP-His8 tagged fusion proteins under control of the *GAL1* promoter. A Tobacco Etch Virus (TEV) protease site between afTMEM16 and the yEGFP-His8 tag allows for tag removal. The afTMEM16 D511A/E514A mutant was generated using the Quickchange method (*Agilent*), and fully sequenced. The vector was transformed into *Saccharomyces cerevisiae* FYG217 competent cells [40] carrying a URA3 deletion for positive selection. Cells were grown in yeast synthetic drop-out medium supplemented with Uracil (CSM-URA, *MP Biomedicals*). Expression was induced with 2% (w/v) galactose at 30°C and monitored by GFP fluorescence detection and western blotting with anti-GFP and anti-His antibodies (*Santa Cruz biotechnology*). Cells were collected after 22 h and lysed in an EmulsiFlex-C5 homogenizer at 25,000 psi in buffer P (150 mM KCl, 10% (w/v) glycerol, 50 mM Tris-HCl, pH 8) supplemented with 1 mM EDTA, 5 µg/ml leupeptin, 2 µg/ml pepstatin, 100 µM phenylmethane sulphonylfluoride (PMSF) and protease inhibitor cocktail tablets (*Roche*). Extraction was carried out by adding digitonin (*EMD Biosciences*) for afTMEM16 and Foscholine 12 (*Affymetrix*) for Ist2p, to 1%

(w/v) for 1–2 h at 4°C with gentle mixing. After centrifugation at 40,000 *g*for 45 min, 1 mM $MgCl_2$ and 10 mM Imidazole were added, the supernatant was loaded on a Ni-NTA agarose resin (*Qiagen*), washed with buffer P+ 30 mM Imidazole and 0.12% (w/v) digitonin (0.1% w/v Foscholine 12 for Ist2p) and eluted with buffer P +300 mM Imidazole and 0.12% (w/v) digitonin (0.1% w/v Foscholine 12 for Ist2p). After overnight treatment with TEV protease to remove the His-tag, the protein was run on a Superdex 200 column (*GE Healthcare*) with buffer P containing 0.12% (w/v) digitonin (0.1% w/v Foscholine 12 for Ist2p) and the peak fraction containing afTMEM16 was collected.

Liposome preparation

Liposomes were formed in E. coli polar extract:Egg PC (60%) (3:1) or in 100% E. coli polar extra (all from *Avanti Polar Lipid*) unless otherwise noted. Lipids were dissolved in buffer L (300 mM KCl, 50 mM HEPES, 0.5 mM $Ca(NO_3)_2$ or 1 mM EGTA, pH 7.4) (unless otherwise stated) and 35 mM CHAPS. Purified protein was added to the detergent/lipid suspension to the desired protein density (5 µg protein/mg lipid unless otherwise stated). Detergent was removed by using Bio-beads (4 changes of 200 mg Bio-beads SM-2 adsorbent (*Bio-Rad*)/ml of liposomes pre-equilibrated with buffer L and incubated at 4°C with gentle rotation for 48 hours) or by dialysis (4 changes at 1000x volume of buffer L over 36 hours at 4°C). Liposomes were collected, flash frozen in liquid nitrogen and stored at -80°C. Both methods gave comparable results in both Cl^- flux and lipid scrambling assays.

Preparation of the Ca^{2+} solutions

The free [Ca^{2+}] present in our standard solution (300 mM KCl, 50 mM HEPES, pH 7.4) was measured with a Ca-sensitive electrode (Orion Research, Inc.), and found to be 55±5 μM. The amounts of Ca^{2+} and EGTA to generate the desired free Ca^{2+} concentrations were calculated using the program Ca-EGTA Calculator v1.3, from the website (http://www.stanford.edu/~cpatton/CaEGTA-TS.htm) and the values were verified (for $[Ca^{2+}]_{free}$>1 μM) using the Ca-sensitive electrode. For solutions containing less than 1 μM $[Ca^{2+}]_{free}$the predicted value was used. Our 0 mM Ca^{2+} solution was obtained by adding 1 mM EGTA to the standard solution for a predicted $[Ca^{2+}]_{free}$ of ~8 nM.

Flux assay

Liposomes were extruded through a 400 nm membrane filter and centrifuged through a Sephadex G-50 column (*Sigma-Aldrich*) pre-equilibrated in the desired external buffer (1 mM KCl, 300 mM Na-glutamate, 50 mM HEPES pH 7.4, 0.5 mM $Ca(NO_3)_2$ or 1mM EGTA). 100 μl of liposomes were diluted in 2 ml of buffer and the Cl^-time course was monitored with an AgCl electrode. After baseline stabilization, 1 μl of the K^+ ionophore Valinomycin (2 mg/ml) was added to test whether Cl^- efflux could be initiated. The experiment was terminated after 90s by addition of 40 μl of 1.5 M n-octyl-β-D-glucopyranoside (*Affymetrix*) to dissolve liposomes and determine the total Cl^- content of the liposomes, ΔCl^-. For each experiment, ΔCl^- was normalized to the average Cl^- content of 3+ experiments

with protein-free liposomes in the presence of 0.5 mM Ca^{2+}prepared from the same batch of lipids.

Planar lipid bilayer recordings

Horizontal planar lipid bilayers [115] were formed from decane solutions of POPE/POPG or E. Coli/Egg PC lipids at 10 mg/ml. The *cis* chamber contained 300 mM KCl, 20 mM HEPES, 0.5 mM $Ca(NO_3)_2$, pH 7.4 and the *trans* chamber contained 30 mM KCl, 20 mM HEPES, 0.5 mM $Ca(NO_3)_2$, pH 7.4. Proteoliposomes (in the presence of 0.5 mM $Ca(NO_3)_2$ were sonicated for 5 s and 1 µl was added to the *cis* chamber. Bilayer formation was monitored by measuring the capacity using a triangular wave; acceptable capacities were 70-110 pF. After addition of 1 µL of liposomes, 1 µL of 3 M KCl was added to promote fusion. Successful incorporation of channels was monitored by holding at -100 or +100 mV. Bilayer capacity was periodically checked. The minimum wait time for channel incorporation was 10 minutes. Bilayers formed from the E. Coli/Egg PC mix proved to be unstable and on average lasted < 5 min from formation. Currents were recorded using the GePulse software (*by M. Pusch, Istituto di Biofisica, Genova, Italy*) with a Whole Cell/Patch Clamp Amplifier PC-505B (*Warner Instruments*) sampled at 1 ms and filtered at 1 kHz.

Lipid Scrambling

Liposomes were prepared as described above, except that trace amounts of nitrobenzoxadiazole-phospholipid (NBD-PL) (0.5 mole %) were included.

Scrambling activity was assayed as described previously [11]. Briefly, liposomes were loaded with 300 mM KCl and 50 mM HEPES pH 7.4. Ca^{2+} concentrations were adjusted as described above by adding Ca2+ or EGTA by freeze/thaw cycles. Liposomes were extruded through a 400 nm membrane filter and 20 µl were diluted to 2 ml in 300 mM KCl, 50 mM HEPES, X mM $Ca(NO_3)_2$ OR 1mM EGTA, pH 7.4 in a stirred cuvette at 23°C and the fluorescence intensity (excitation 470 nm, emission 530 nm) was recorded in a PTI spectrofluorimeter. 40 µl of sodium dithionite (40 mM final concentration) or fatty-acid-free BSA (1.5 mg/ml final concentration) were added to the cuvette to start the reaction. Data was collected using *FelixGX 4.1.0* at a sampling rate of 1 or 10 Hz.

Analysis of the time course of fluorescence decay

The general form of the model describing the dithionite-induced fluorescence decay of proteoliposomes containing a single scramblase is a three state scheme

$$L^*_{in} \underset{\kappa_{-1}}{\overset{\kappa_{+1}}{\rightleftarrows}} L^*_{out} \xrightarrow{\kappa_2} L \qquad \text{(Eq. 1)}$$

Where $L^*_{in/out}$ denote the fluorescent form of the lipid in the inner (outer) leaflet and L is the dithionite-reduced non-fluorescent form, $\kappa_{\pm 1}$ are the forward and backwards rate of scrambling and κ_2 is the rate of dithionite reduction. Since this is a three-state system the time evolution of $L^*_{in}(t)$, $L^*_{out}(t)$ and L(t) is described by a double exponential [116]. The time course of the normalized fluorescence is

$$\frac{F(t)}{F_{max}} = \frac{L^*_{in}(t)+L^*_{out}(t)}{L^*_{in}(t=0)+L^*_{out}(t=0)} \qquad \text{(Eq.2)}$$

Which was fit to:

$$F/F_{Max} = A_0 + A_{Fast}e^{-t/\tau_{Fast}} + A_{Slow}e^{-t/\tau_{Slow}} \quad \text{(Eq. 3)}$$

Where A_0 is an offset needed to account for the fraction of refractory liposomes, $A_{Fast(Slow)}$ is the relative weight of the fast (slow) component of the decay and $\tau_{Fast(Slow)}$ is its relative time constant. It is important to note that $A_{Fast(Slow)}$ and $\tau_{Fast(Slow)}$ are complex functions of the rates of scrambling and of dithionite reduction and therefore do not represent distinct physical processes. For $[Ca^{2+}] <$ 1 μM the trace is well fit with a double exponential. For $[Ca^{2+}] >$ 5 μM the process is well described by a single exponential as A_{Slow} becomes ~0.

Poisson analysis

Assuming that the reconstitution process randomly inserts proteins into liposomes, the fraction of liposomes containing 0 copies of a protein, f_0, is given by Poisson statistics

$$f_0 = e^{-N_P/N_L} = e^{-p/p_0} \quad \text{(Eq. 4)}$$

where N_P and N_L are the number of proteins and liposomes in the sample, p is the protein density, $p_0 = \frac{\gamma M_p}{\varphi N_A}$, γ is the number of liposomes per mass of lipid, M_P is the mass of the functional protein complex, φ is the fraction of active proteins and N_A is Avogadro's number [102]. In our analysis we assumed that φ~1 and used the experimentally derived values of γ reported in the literature [102].

To compare the f_0 values obtained from assays with different dynamical ranges (fluxes, dithionite and scrambling) the data was normalized as follows

$$f_0^{norm} = \frac{y_{max} - y}{y_{max} - y_0} \cdot 100 \quad \text{(Eq. 5)}$$

where y_0 is the signal measured with protein-free liposomes, y_{max} is the signal at 5 µg protein/mg lipid and y is the signal measured at each protein concentration.

Data analysis and statistics

Data were analyzed using the Ana software (*by M. Pusch, Istituto di Biofisica, Genova, Italy*), Microsoft excel and SigmaPlot 10.0. The experiments were repeated at least 3 times, exact numbers are reported in the text or in the figure legends. Data points are reported as mean±S.E.M. The error reported for parameters derived from fits is the uncertainty of the fit rather than the S.E.M.

NBD-labelled PEG-conjugated phospholipid synthesis

The synthesis of NBD-labelled PEG phospholipids was done by our collaborators in the laboratory of Dr. Anant Menon (in particular by Rabia Iqbal and Ashley Brown). Synthesis of 1,2-distearoyl-*sn*-glycero-3-phosphoethanolamine-*N*-polyethylene glycol-X-(7-Nitrobenz-2-Oxa-1,3-Diazol-4-yl) or (DSPE PEG NBD). This synthesis involved conjugating the fluorescent NBD-X-succinimidyl ester (SE) to DSPE PEG amine via an amide linkage, with loss of *N*-hydroxysuccinimide (NHS). The size of the PEG molecules is 1000-10000. The resulting product was verified by Thin Layer Chromatography (TLC) and Electro Spray Ionization Mass Spectroscopy (ESI-MS).

Conjugation was achieved by dissolving DSPE PEG amine (9.8 mg, 0.0035 mmol) in anhydrous CH_2Cl_2 (1.5 mL) (***1***). This was followed by addition of triethylamine (0.01 mL) and NBD-X, SE (2.7 mg, 0.0070 mmol) (***2***). The reaction

was stirred 1 h under N_2. Reaction progress was monitored by TLC using silica gel 6050 plates with 85% $CHCl_3$/MeOH, eluting three times each. TLC analysis showed a new fluorescent spot corresponding to the expected product. The crude was dried under N_2 and the product was purified by prep TLC with 85% $CHCl_3$/MeOH, eluted three times to separate out impurities, appearing as minor fluorescent spots. The middle fluorescent band, corresponding to the product, was scraped off from the TLC plate using a spatula and collected into a medium sized fritted glass funnel with a glass wool plug. The product (***3***) was recovered by vacuum filtration, with several washes of 50 % $CHCl_3$/MeOH. The product was obtained in 54% yield (5.8 mg, 0.0019 mmol).

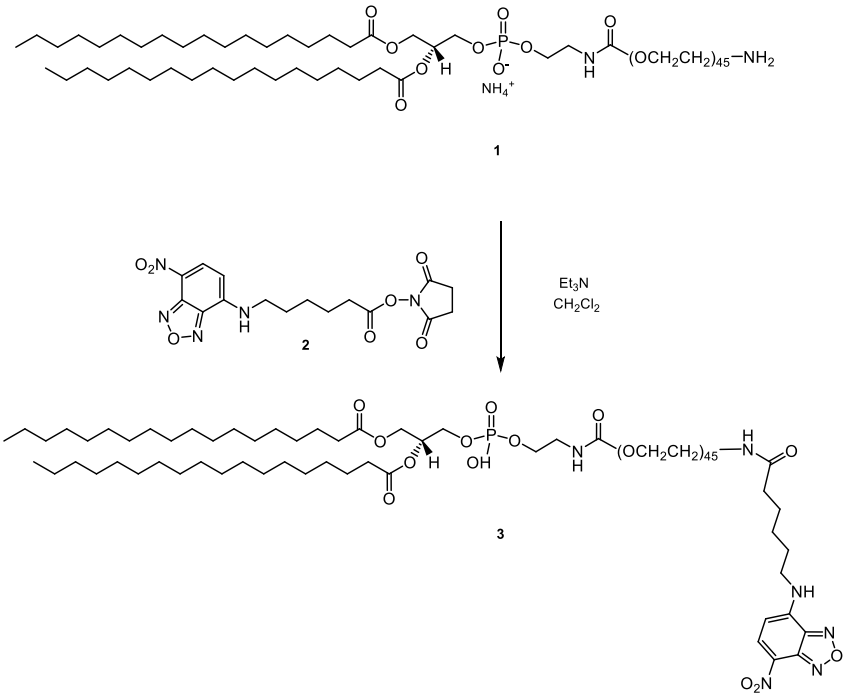

Dynamic Light Scattering

Analysis of PEG size was performed by Light Scattering after separation by methanolysis under basic conditions. At least 1 mg of DSPE PEG NBD was dissolved in methanol (0.9 mL) and transfered into a glass reconstitution tube.

Upon addition of 10.0 M NaOH (0.1 mL) the sample was incubated at 60 °C for 3-4 h (without stirring), dried down under nitrogen and resuspended in chloroform. The product was separated by TLC, collected into a fritted glass funnel, recovered by vacuum filtration with several washes of 1:1 chloroform/methanol (v/v) and transferred to a tared round bottom flask. The product was then dried down, resuspended in methanol to make a 1 mg/mL solution and centrifuged for 15 min at 8000 rpm at 4 °C. Supernatant was collected and DLS measurements were performed (*Malvern Instruments, Zetasizer Nano-S*) at 25 °C with 0 second delay. The sample was clarified prior the experiment. A dust-free quartz cuvette was used.

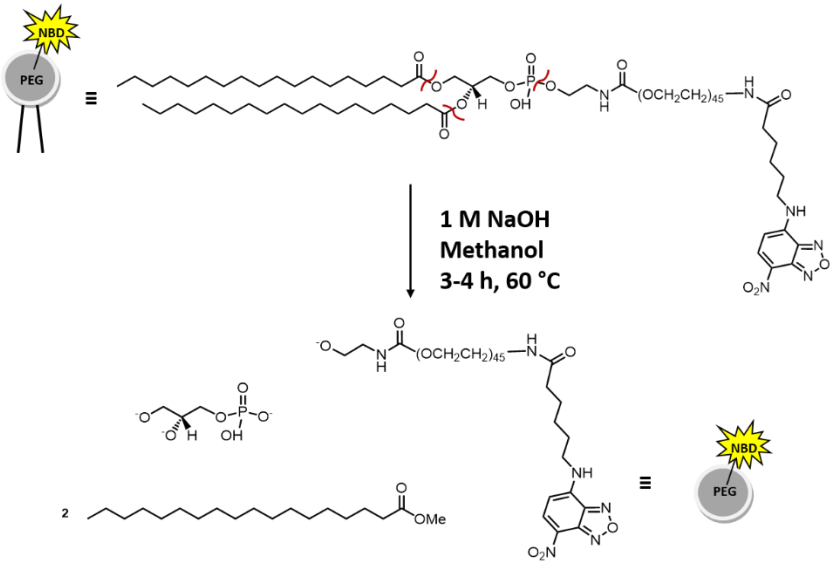

8. Bibliography

1 Clark, M. R. Flippin' lipids. *Nature immunology* **12**, 373-375, doi:10.1038/ni.2024 (2011).

2 Eckford, P. D. & Sharom, F. J. The reconstituted Escherichia coli MsbA protein displays lipid flippase activity. *The Biochemical journal* **429**, 195-203, doi:10.1042/BJ20100144 (2010).

3 Quazi, F. & Molday, R. S. Differential phospholipid substrates and directional transport by ATP-binding cassette proteins ABCA1, ABCA7, and ABCA4 and disease-causing mutants. *The Journal of biological chemistry* **288**, 34414-34426, doi:10.1074/jbc.M113.508812 (2013).

4 Eckford, P. D. & Sharom, F. J. The reconstituted P-glycoprotein multidrug transporter is a flippase for glucosylceramide and other simple glycosphingolipids. *The Biochemical journal* **389**, 517-526, doi:10.1042/BJ20050047 (2005).

5 Wang, L., Beserra, C. & Garbers, D. L. A novel aminophospholipid transporter exclusively expressed in spermatozoa is required for membrane lipid asymmetry and normal fertilization. *Developmental biology* **267**, 203-215, doi:10.1016/j.ydbio.2003.11.004 (2004).

6 Lopez-Marques, R. L. *et al.* Structure and mechanism of ATP-dependent phospholipid transporters. *Biochimica et biophysica acta* **1850**, 461-475, doi:10.1016/j.bbagen.2014.04.008 (2015).

7 Perez, C. *et al.* Structure and mechanism of an active lipid-linked oligosaccharide flippase. *Nature* **524**, 433-438, doi:10.1038/nature14953 (2015).

8 Kornberg, R. D. & McConnell, H. M. Inside-outside transitions of phospholipids in vesicle membranes. *Biochemistry* **10**, 1111-1120 (1971).

9 Bai, J. & Pagano, R. E. Measurement of spontaneous transfer and transbilayer movement of BODIPY-labeled lipids in lipid vesicles. *Biochemistry* **36**, 8840-8848, doi:10.1021/bi970145r (1997).

10 Bevers, E. M. & Williamson, P. L. Phospholipid scramblase: an update. *FEBS Lett.* **584**, 2724-2730 (2010).

11 Menon, I. *et al.* Opsin is a phospholipid flippase. . *Curr Biol.* **21**, 149-153 (2011).

12 Bevers, E. M. & Williamson, P. L. in *Transmembrane Dynamics of Lipids* (eds P. Devaux & A. Herrmann) 119-146 (Wiley, 2011).

13 Balasubramanian, K. & Schroit, A. J. Aminophospholipid asymmetry: A matter of life and death. *Annu Rev Physiol* **65** (2003).

14 Segawa, K., Suzuki, J. & Nagata, S. Constitutive exposure of phosphatidylserine on viable cells. *PNAS* **108**, 19246-19251 (2011).

15 van den Eijnde, S. M. *et al.* Transient expression of phosphatidylserine at cell-cell contact areas is required for myotube formation. *J Cell Sci* **114**, 3631-3642 (2001).

16 Bell, R. M., Hannun, Y. A. & Loomis, C. R. Mechanism of regulation of protein kinase C by lipid second messengers. *Symposium on Fundamental Cancer Research* **39**, 145-156 (1986).

17 Chandra, R., Joshi, P. C., Bajpai, V. K. & Gupta, C. M. Membrane phospholipid organization in calcium-loaded human erythrocytes. *Biochim Biophys Acta.* **902**, 253-262 (1987).

18 Connor, J., Gillum, K. & Schroit, A. J. Maintenance of lipid asymmetry in red blood cells and ghosts: effect of divalent cations and serum albumin on the transbilayer distribution of phosphatidylserine. *Biochimica et biophysica acta* **1025**, 82-86 (1990).

19 Hampton, M. B., Vanags, D. M., Porn-Ares, M. I. & Orrenius, S. Involvement of extracellular calcium in phosphatidylserine exposure during apoptosis. *FEBS letters* **399**, 277-282 (1996).

20 Bratton, D. L. *et al.* Appearance of phosphatidylserine on apoptotic cells requires calcium-mediated nonspecific flip-flop and is enhanced by loss of the aminophospholipid translocase. *The Journal of biological chemistry* **272**, 26159-26165 (1997).

21 Comfurius, P. *et al.* Reconstitution of phospholipid scramblase activity from human blood platelets. *Biochemistry* **35**, 7631-7634 (1996).

22 Bassé, F., Stout, J. G., Sims, P. J. & Wiedmer, T. Isolation of an erythrocyte membrane protein that mediates Ca2+-dependent transbilayer movement of phospholipid. *The Journal of biological chemistry* **271**, 17205-17210 (1996).

23 Hamon, Y. *et al.* ABC1 promotes engulfment of apoptotic cells and transbilayer redistribution of phosphatidylserine. *Nature cell biology* **2**, 399-406, doi:10.1038/35017029 (2000).

24 Ravichandran, K. S. Find-me and eat-me signals in apoptotic cell clearance: progress and conundrums. *The Journal of experimental medicine* **207**, 1807-1817, doi:10.1084/jem.20101157 (2010).

25 Yang, Y. D. *et al.* TMEM16A confers receptor-activated calcium-dependent chloride conductance. *Nature* **455**, 6 (2008).

26 Caputo, A. *et al.* TMEM16A, a membrane protein associated with calcium-dependent chloride channel activity. *Science* **322**, 5 (2008).

27 Schroeder, B. C., Cheng, T., Jan, Y. N. & Jan, L. Y. Expression cloning of TMEM16A as a calcium-activated chloride channel subunit. *Cell* **134**, 11 (2008).

28 Stohr, H. *et al.* TMEM16B, a novel protein with calcium-dependent chloride channel activity, associates with a presynaptic protein complex in photoreceptor

terminals. *The Journal of neuroscience : the official journal of the Society for Neuroscience* **29**, 6809-6818, doi:10.1523/JNEUROSCI.5546-08.2009 (2009).

29 Suzuki, J., Umeda, M., Sims, P. J. & Nagata, S. Calcium-dependent phospholipid scrambling by TMEM16F. *Nature* **468**, 834-838 (2010).

30 Scudieri, P. *et al.* Ion channel and lipid scramblase activity associated with expression of TMEM16F/ANO6 isoforms. *The Journal of physiology* **593**, 3829-3848, doi:10.1113/JP270691 (2015).

31 Yu, K. *et al.* Identification of a lipid scrambling domain in ANO6/TMEM16F. *eLife* **4**, e06901, doi:10.7554/eLife.06901 (2015).

32 Suzuki, J. *et al.* Calcium-dependent Phospholipid Scramblase Activity of TMEM16 Family Members. *The Journal of biological chemistry* **288**, 13305-13316 (2013).

33 Brunner, J. D., Lim, N. K., Schenck, S., Duerst, A. & Dutzler, R. X-ray structure of a calcium-activated TMEM16 lipid scramblase. *Nature* **516**, 207-212 (2014).

34 Guindon, S. *et al.* New algorithms and methods to estimate maximum-likelihood phylogenies: assessing the performance of PhyML 3.0. *Syst Biol* **59**, 307-321 (2010).

35 Gouy, M., Guindon, S. & Gascuel, O. SeaView version 4: A multiplatform graphical user interface for sequence alignment and phylogenetic tree building. *Mol Biol Evol* **27**, 221-224 (2010).

36 Picollo, A., Malvezzi, M. & Accardi, A. TMEM16 Proteins: Unknown Structure and Confusing Functions. *J Mol Bio* **427**, 94-105 (2015).

37 Zwaal, R. F., Comfurius, P. & Bevers, E. M. Scott syndrome, a bleeding disorder caused by defective scrambling of membrane phospholipids. *Biochim Biophys Acta.* **1636**, 119-128 (2004).

38 Castoldi, E., Collins, P. W., Williamson, P. L. & Bevers, E. M. Compound heterozygosity for 2 novel TMEM16F mutations in a patient with Scott syndrome. *Blood* **117**, 4399-4400 (2011).

39 Mizuta, K. *et al.* Molecular characterization of GDD1/TMEM16E, the gene product responsible for autosomal dominant gnathodiaphyseal dysplasia. *Biochemical and biophysical research communications* **357**, 126-132, doi:10.1016/j.bbrc.2007.03.108 (2007).

40 Tsutsumi, S. *et al.* The novel gene encoding a putative transmembrane protein is mutated in gnathodiaphyseal dysplasia (GDD). *American journal of human genetics* **74**, 1255-1261 (2004).

41 Sousa, S. B. *et al.* Gain-of-function mutations in the phosphatidylserine synthase 1 (PTDSS1) gene cause Lenz-Majewski syndrome. *Nature genetics* **46**, 70-76, doi:10.1038/ng.2829 (2014).

42 Bolduc, V. *et al.* Recessive mutations in the putative calcium-activated chloride channel Anoctamin 5 cause proximal LGMD2L and distal MMD3 muscular dystrophies. *American journal of human genetics* **86**, 213-221 (2010).

43 Hicks, D. *et al.* A founder mutation in Anoctamin 5 is a major cause of limb-girdle muscular dystrophy. *Brain* **134**, 171-182 (2011).

44 Mahjneh, I. *et al.* A new distal myopathy with mutation in anoctamin 5. *Neuromuscul Disord* **20**, 791-795 (2010).

45 Vermeer, S. *et al.* Targeted next-generation sequencing of a 12.5 Mb homozygous region reveals ANO10 mutations in patients with autosomal-recessive cerebellar ataxia. *American journal of human genetics* **87**, 813-819, doi:10.1016/j.ajhg.2010.10.015 (2010).

46 Chamova, T. *et al.* ANO10 c.1150_1151del is a founder mutation causing autosomal recessive cerebellar ataxia in Roma/Gypsies. *Journal of neurology* **259**, 906-911, doi:10.1007/s00415-011-6276-6 (2012).

47 Renaud, M. *et al.* Autosomal recessive cerebellar ataxia type 3 due to ANO10 mutations: delineation and genotype-phenotype correlation study. *JAMA neurology* **71**, 1305-1310, doi:10.1001/jamaneurol.2014.193 (2014).

48 Sawada, K. *et al.* Striking pattern of Purkinje cell loss in cerebellum of an ataxic mutant mouse, tottering. *Acta neurobiologiae experimentalis* **69**, 138-145 (2009).

49 Zech, M. *et al.* Rare sequence variants in ANO3 and GNAL in a primary torsion dystonia series and controls. *Movement disorders : official journal of the Movement Disorder Society* **29**, 143-147, doi:10.1002/mds.25715 (2014).

50 Huang, F. *et al.* TMEM16C facilitates Na+-activated K+ currents in rat sensory neurons and regulates pain processing. *Nat Neurosci* **Published online 21 July 2013** (2013).

51 Miwa, S., Nakajima, T., Murai, Y., Takano, Y. & Sugiyama, T. Mutation assay of the novel gene DOG1 in gastrointestinal stromal tumors (GISTs). *J Gastroenterol* **43**, 7 (2008).

52 Espinosa, I. *et al.* A novel monoclonal antibody against DOG1 is a sensitive and specific marker for gastrointestinal stromal tumors. *Am J Surg Pathol* **32**, 210-218 (2008).

53 Huang, X., Gollin, S. M., Raja, S. & Godfrey, T. E. High-resolution mapping of the 11q13 amplicon and identification of a gene, TAOS1, that is amplified and overexpressed in oral cancer cells. *Proceedings of the National Academy of Sciences of the United States of America* **99**, 11369-11374, doi:10.1073/pnas.172285799 (2002).

54 Duvvuri, U. *et al.* TMEM16A Induces MAPK and Contributes Directly to Tumorigenesis and Cancer Progression. *Cancer research* **72**, 3270-3281 (2012).

55 Liu, F. *et al.* TMEM16A overexpression contributes to tumor invasion and poor prognosis of human gastric cancer through TGF-beta signaling. *Oncotarget* **6**, 11585-11599, doi:10.18632/oncotarget.3412 (2015).

56 Sui, Y. *et al.* Inhibition of TMEM16A expression suppresses growth and invasion in human colorectal cancer cells. *PloS one* **9**, e115443, doi:10.1371/journal.pone.0115443 (2014).

57 Bera, T. K. *et al.* NGEP, a gene encoding a membrane protein detected only in prostate cancer and normal prostate. *Proceedings of the National Academy of Sciences of the United States of America* **101**, 3059-3065 (2004).

58 Das, S. *et al.* Topology of NGEP, a prostate-specific cell:cell junction protein widely expressed in many cancers of different grade level. *Cancer research* **68**, 6306-6312 (2008).

59 Das, S. *et al.* NGEP, a prostate-specific plasma membrane protein that promotes the association of LNCaP cells. *Cancer research* **67**, 1594-1601, doi:10.1158/0008-5472.CAN-06-2673 (2007).

60 Miledi, R. A calcium-dependent transient outward current in Xenopus laevis oocytes. *Proc R Soc Lond B Biol Sci* **215**, 491-497 (1982).

61 Barish, M. E. A transient calcium-dependent chloride current in the immature Xenopus oocyte. *J. Physiol.* **342**, 309-325 (1983).

62 Bader, C. R., Bertrand, D. & Schwartz, E. A. Voltage-activated and calcium-activated currents studied in solitary rod inner segments from the salamander retina. *The Journal of physiology* **331**, 253-284 (1982).

63 Kunzelmann, K., Milenkovic, V. M., Spitzner, M., Soria, R. B. & Schreiber, R. Calcium-dependent chloride conductance in epithelia: is there a contribution by

Bestrophin? *Pflugers Archiv : European journal of physiology* **454**, 879-889, doi:10.1007/s00424-007-0245-z (2007).

64 Guo, D. *et al.* Calcium-activated chloride current contributes to action potential alternations in left ventricular hypertrophy rabbit. *Am J Physiol Heart Circ Physiol* **295**, H97-H104 (2008).

65 Andre, S. *et al.* Axotomy-Induced Expression of Calcium-Activated Chloride Current in Subpopulations of Mouse Dorsal Root Ganglion Neurons. *J Neurophysiol* **90**, 3764-3773 (2003).

66 Reisert, J., Bauer, P. J., Yau, K. W. & Frings, S. The Ca-activated Cl channel and its control in rat olfactory receptor neurons. *The Journal of general physiology* **122**, 349-363 (2003).

67 Angermann, J. E., Sanguinetti, A. R., Kenyon, J. L., Leblanc, N. & Greenwood, I. A. Mechanism of the inhibition of Ca2+-activated Cl- currents by phosphorylation in pulmonary arterial smooth muscle cells. *The Journal of general physiology* **128**, 73-87, doi:10.1085/jgp.200609507 (2006).

68 Lalonde, M. R., Kelly, M. E. & Barnes, S. Calcium-activated chloride channels in the retina. *Channels* **2**, 252-260 (2008).

69 Sanchez-Vives, M. V. & Gallego, R. Calcium-dependent chloride current induced by axotomy in rat sympathetic neurons. *The Journal of physiology* **475**, 391-400 (1994).

70 Terashima, H., Picollo, A. & Accardi, A. Purified TMEM16A is sufficient to form Ca2+ activated Cl- channels. *Proceedings of the National Academy of Sciences of the United States of America* **110**, 19354-19359 (2013).

71 Huang, F. *et al.* Studies on expression and function of the TMEM16A calcium-activated chloride channel. *Proceeding of the National Academy of Sciences USA* **106**, 21413-21418 (2009).

72 Ousingsawat, J. *et al.* Loss of TMEM16A causes a defect in epithelial Ca2+-dependent chloride transport. *The Journal of biological chemistry* **284**, 28698-28703, doi:10.1074/jbc.M109.012120 (2009).

73 Rock, J. R. *et al.* Transmembrane Protein 16A (TMEM16A) Is a Ca2+-regulated Cl- Secretory Channel in Mouse Airways. *The Journal of biological chemistry* **284**, 14875-14880 (2009).

74 Reyes, J. P. *et al.* Anion permeation in calcium-activated chloride channels formed by TMEM16A from Xenopus tropicalis. *Pflugers Archiv : European journal of physiology* **466**, 1769-1777 (2014).

75 Yu, K., Duran, C., Qu, Z., Cui, Y. Y. & Hartzell, H. C. Explaining calcium-dependent gating of anoctamin-1 chloride channels requires a revised topology. . *Circ. Res* **110**, 990-999 (2012).

76 Yu, K., Zhu, J., Qu, Z., Cui, Y. Y. & Hartzell, H. C. Activation of the Ano1 (TMEM16A) chloride channel by calcium is not mediated by calmodulin. *The Journal of general physiology* **143**, 253-267 (2014).

77 Yang, H. *et al.* TMEM16F Forms a Ca(2+)-Activated Cation Channel Required for Lipid Scrambling in Platelets during Blood Coagulation. *Cell* **151**, 111-122 (2012).

78 Pifferi, S., Dibattista, M. & Menini, A. TMEM16B induces chloride currents activated by calcium in mammalian cells. *Pflugers Archiv : European journal of physiology* **458**, 1023-1038 (2009).

79 Stephan, A. B., . *et al.* ANO2 is the cilial calcium-activated chloride channel that may mediate olfactory amplification. *Proceedings of the National Academy of Sciences of the United States of America* **106**, 11776-11781 (2009).

80 Kmit, A. *et al.* Calcium-activated and apoptotic phospholipid scrambling induced by Ano6 can occur independently of Ano6 ion currents. *Cell Death Dis* **4** (2013).

81 van Kruchten, R. *et al.* Both TMEM16F-dependent and TMEM16F-independent pathways contribute to phosphatidylserine exposure in platelet apoptosis and platelet activation. *Blood* **10.1182/blood-2012-09-454314** (2013).

82 Ehlen, H. W. *et al.* Inactivation of Anoctamin-6/Tmem16f, a regulator of phosphatidylserine scrambling in osteoblasts, leads to decreased mineral deposition in skeletal tissues. *J Bone Miner Res* **28**, 246-259 (2012).

83 Ousingsawat, J. *et al.* Anoctamin-6 controls bone mineralization by activating the calcium transporter NCX1. *The Journal of biological chemistry* **290**, 6270-6280, doi:10.1074/jbc.M114.602979 (2015).

84 Almaca, J. *et al.* TMEM16 proteins produce volume-regulated chloride currents that are reduced in mice lacking TMEM16A. . *The Journal of biological chemistry* **284**, 28571-28578 (2009).

85 Martins, J. R. *et al.* Anoctamin 6 is an essential component of the outwardly rectifying chloride channel. *PNAS* **108**, 18168-18172 (2011).

86 Kunzelmann, K. *et al.* Expression and function of epithelial anoctamins. . *Exp Physiol* **97**, 184-192 (2012).

87 Grubb, S. *et al.* TMEM16F (Anoctamin 6), an anion channel of delayed Ca2+ activation. *The Journal of general physiology* **141**, 585-600 (2013).

88 Tian, Y., Schreiber, R. & Kunzelmann, K. Anoctamins are a family of Ca2+-activated Cl- channels. *J. Cell Sci.* **125**, 4991-4998 (2012).

89 Shimizu, T. *et al.* TMEM16F is a component of a Ca2+-activated Cl- channel but not a volume-sensitive outwardly rectifying Cl- channel. *Am J Physiol Cell Physiol* **304**, C748-759 (2013).

90 Duran, C., Qu, Z., Osunkoya, A. O., Cui, Y. & Hartzell, H. C. ANOs 3-7 in the anoctamin/Tmem16 Cl- channel family are intracellular proteins. *Am J Physiol Cell Physiol* **302**, C482-493 (2012).

91 Wong, X. M., Younger, S., Peters, C. J., Jan, Y. N. & Jan, L. Y. Subdued, a TMEM16 family Ca2+-activated Cl- channel in Drosophila melanogaster with an unexpected role in host defense. *eLife* **2**, e00862, doi:10.7554/eLife.00862 (2013).

92 Franz, A., Maass, K. & Seedorf, M. A complex peptide-sorting signal, but no mRNA signal, is required for the Sec-independent transport of Ist2 from the yeast ER to the plasma membrane. *FEBS letters* **581**, 401-405 (2007).

93 Manford, A. G., Stefan, C. J., Yuan, H. L., Macgurn, J. A. & Emr, S. D. ER-to-plasma membrane tethering proteins regulate cell signaling and ER morphology. *Developmental cell* **23**, 1129-1140, doi:10.1016/j.devcel.2012.11.004 (2012).

94 Fallah, G. *et al.* TMEM16A(a)/anoctamin-1 shares a homodimeric architecture with CLC chloride channels. *Mol Cell Proteomics* **10**, M110.004697 (2011).

95 Tien, J., Lee, H. Y., Minor, D. L. J., Jan, Y. N. & Jan, L. Y. Identification of a dimerization domain in the TMEM16A calcium-activated chloride channel (CaCC). *Proceedings of the National Academy of Sciences of the United States of America* **110**, 6352-6357 (2013).

96 Xiao, Q. *et al.* Voltage- and calcium-dependent gating of TMEM16A/Ano1 chloride channels are physically coupled by the first intracellular loop. *Proceedings of the National Academy of Sciences of the United States of America* **108**, 8891-8896 (2011).

97 Whitlock, J. M. & Hartzell, H. C. A Pore Idea: the ion conduction pathway of TMEM16/ANO proteins is composed partly of lipid. *Pflugers Archiv : European journal of physiology*, doi:10.1007/s00424-015-1777-2 (2016).

98 Malvezzi, M. *et al.* Ca2+-dependent phospholipid scrambling by a reconstituted TMEM16 ion channel. *Nature Communications* **10.1038/ncomms3367** (2013).

99 McIntyre, J. C. & Sleight, R. G. Fluorescence assay for phospholipid membrane asymmetry. *Biochemistry* **30**, 11819-11827 (1991).

100 Mimms, L. T., Zampighi, G., Nozaki, Y., Tanford, C. & Reynolds, J. A. Phospholipid vesicle formation and transmembrane protein incorporation using octyl glucoside. *Biochemistry* **20**, 833-840 (1981).

101 Chang, Q. L., Gummadi, S. N. & Menon, A. K. Chemical modification identifies two populations of glycerophospholipid flippase in rat liver ER. *Biochemistry* **43**, 10710-10718 (2004).

102 Walden, M. *et al.* Uncoupling and turnover in a Cl^-/H^+ exchange transporter. *J. Gen. Physiol.* **129**, 317-329 (2007).

103 Szoka, F. C. J. & Papahadjopoulos, D. Comparative properties and methods of prepraration of lipid vesicles (liposomes). *Ann. Rev. Biophys. Bioeng.* **9**, 467-508 (1980).

104 Silvius, J. R. Solubilization and functional reconstitution of biomembrane components. *Annu Rev Biophys Biomol Struct* **21**, 323-348 (1992).

105 Kol, M. A., van Dalen, A., de Kroon, A. I. & de Kruijff, B. Translocation of phospholipids is facilitated by a subset of membrane-spanning proteins of the bacterial cytoplasmic membrane. *The Journal of biological chemistry* **278**, 24586-24593 (2003).

106 Sanyal, S., Frank, C. G. & Menon, A. K. Distinct flippases translocate glycerophospholipids and oligosaccharide diphosphate dolichols across the endoplasmic reticulum. . *Biochemistry* **47**, 7937-7946 (2008).

107 Sheridan, J. T. *et al.* Characterization of the oligomeric structure of the Ca(2+)-activated Cl- channel Ano1/TMEM16A. *The Journal of biological chemistry* **286**, 1381-1388 (2011).

108 Hille, B. *Ion channels of excitable membranes*. 3rd edn, (Sinauer, 2001).

109 Ferrera, L. *et al.* A minimal isoform of the TMEM16A protein associated with chloride channel activity. *Biochimica et biophysica acta* **1808**, 2214-2223 (2011).

110 Newman, M. J. & Wilson, T. H. Solubilization and reconstitution of the lactose transport system from Escherichia coli. *The Journal of biological chemistry* **255**, 10583-10586 (1980).

111 Stuart, L. J., Buck, J. P., Tremblay, A. E. & Buist, P. H. Configurational analysis of cyclopropyl fatty acids isolated from Escherichia coli. *Organic letters* **8**, 79-81, doi:10.1021/ol052550d (2006).

112 Tien, J. *et al.* A comprehensive search for calcium binding sites critical for TMEM16A calcium-activated chloride channel activity. *eLife*, e02772, doi:10.7554/eLife.02772 (2014).

113 Peters, C. J. *et al.* Four basic residues critical for the ion selectivity and pore blocker sensitivity of TMEM16A calcium-activated chloride channels. *Proceedings of the National Academy of Sciences of the United States of America* **112**, 3547-3552, doi:10.1073/pnas.1502291112 (2015).

114 Howard, J. B., McKinnon, J. T., Makarovsky, Y., Lafleur, A. L. & Johnson, M. E. Fullerenes C60 and C70 in flames. *Nature* **352**, 139-141, doi:10.1038/352139a0 (1991).

115 Accardi, A., Kolmakova-Partensky, L., Williams, C. & Miller, C. Ionic currents mediated by a prokaryotic homologue of CLC Cl^- channels. *J. Gen. Physiol.* **123**, 109-119. (2004).

116 Marx, U. *et al.* Rapid flip-flop of phospholipids in endoplasmic reticulum membranes studied by a stopped-flow approach. *Biophys J* **78**, 2628-2640 (2000).